Published for SISSA by Springer

Received: *March 23, 2023*
Revised: *August 30, 2023*
Accepted: *September 11, 2023*
Published: *September 19, 2023*

Measurement of the branching fraction of $D_s^+ \to \tau^+\nu_\tau$ via $\tau^+ \to \mu^+\nu_\mu\bar{\nu}_\tau$

The BESIII collaboration

E-mail: besiii-publications@ihep.ac.cn

Abstract: Utilizing $7.33\,\mathrm{fb}^{-1}$ of e^+e^- collision data taken at the center-of-mass energies of 4.128, 4.157, 4.178, 4.189, 4.199, 4.209, 4.219, and 4.226 GeV with the BESIII detector, the branching fraction of the leptonic decay $D_s^+ \to \tau^+\nu_\tau$ via $\tau^+ \to \mu^+\nu_\mu\bar{\nu}_\tau$ is measured to be $\mathcal{B}_{D_s^+\to\tau^+\nu_\tau} = (5.37 \pm 0.17_{\rm stat} \pm 0.15_{\rm syst})\%$. Combining this branching fraction with the world averages of the measurements of the masses of τ^+ and D_s^+ as well as the lifetime of D_s^+, we extract the product of the decay constant of D_s^+ and the $c \to s$ Cabibbo-Kobayashi-Maskawa matrix element to be $f_{D_s^+}|V_{cs}| = (246.7 \pm 3.9_{\rm stat} \pm 3.6_{\rm syst})$ MeV. Taking $|V_{cs}|$ from a global fit in the standard model we obtain $f_{D_s^+} = (253.4 \pm 4.0_{\rm stat} \pm 3.7_{\rm syst})$ MeV. Conversely, taking $f_{D_s^+}$ from lattice quantum chromodynamics calculations, we obtain $|V_{cs}| = 0.987 \pm 0.016_{\rm stat} \pm 0.014_{\rm syst}$.

Keywords: e^+-e^- Experiments

ArXiv ePrint: 2303.12468

https://doi.org/10.1007/JHEP09(2023)124

Contents

JHEP09(2023)124

1 Introduction

Leptonic decays offer an ideal laboratory for studying strong and weak interaction effects in the charmed meson system. In the standard model (SM) of particle physics, the D_s^+ meson decays into $\ell^+\nu_\ell$ ($\ell = e$, μ or τ) via annihilation mediated by a virtual W^+ boson. Throughout this paper, the inclusion of charge conjugate channels is always implied. The partial width of $D_s^+ \to \ell^+\nu_\ell$ at lowest order can be related to the D_s^+ decay constant $f_{D_s^+}$ via [1]

$$\Gamma_{D_s^+\to\ell^+\nu_\ell} = \frac{G_F^2}{8\pi}|V_{cs}|^2 f_{D_s^+}^2 m_\ell^2 m_{D_s^+}\left(1-\frac{m_\ell^2}{m_{D_s^+}^2}\right)^2, \tag{1.1}$$

where G_F is the Fermi coupling constant, $|V_{cs}|$ is the $c \to s$ Cabibbo-Kobayashi-Maskawa (CKM) matrix element, m_ℓ is the mass of the lepton, and $m_{D_s^+}$ is the mass of the D_s^+ meson. Extraction of $f_{D_s^+}$ in experiments is important for testing various theoretical calculations based on different approaches [2–10]. In recent years, the precision of calculations of $f_{D_s^+}$ based on Lattice Quantum Chromodynamics (LQCD) has reached a level of 0.2% [7], and much progress has been achieved in the experimental studies of $D_s^+ \to \ell^+\nu_\ell$ decays by the

CLEO [11–13], BaBar [14], Belle [15], and BESIII [16, 17, 19–22] collaborations. Based on the average of the branching fractions (BFs) reported by these experiments, one can derive $f_{D_s^+}$ with a precision of 1.0%. Precise and intensive estimations of $f_{D_s^+}$ are still desirable to test theoretical calculations with higher precision. Improved measurements of $f_{D_s} \times |V_{\rm cs}|$ are therefore important for testing the unitarity of the CKM matrix [23] with higher sensitivity.

In the SM, the ratio of the BFs of $D_s^+ \to \tau^+\nu_\tau$ and $D_s^+ \to \mu^+\nu_\mu$ can be written as

$$\mathcal{R}_{\tau/\mu} = \frac{\mathcal{B}_{D_s^+\to\tau^+\nu_\tau}}{\mathcal{B}_{D_s^+\to\mu^+\nu_\mu}} = \frac{m_{\tau^+}^2\left(1-\frac{m_{\tau^+}^2}{m_{D_s^+}^2}\right)^2}{m_{\mu^+}^2\left(1-\frac{m_{\mu^+}^2}{m_{D_s^+}^2}\right)^2}, \tag{1.2}$$

which only depends on the charged lepton and D_s^+ meson masses. Inserting the world averages of m_τ, m_μ, and m_{D_s} [24] in the above equation gives $\mathcal{R}_{\tau/\mu} = 9.75 \pm 0.01$. Measurements of the BFs of $D_s^+ \to \ell^+\nu_\ell$ allow this ratio to be determined experimentally and provide an important test of $\tau - \mu$ lepton flavor universality.

In this paper, we present a measurement of the BF of $D_s^+ \to \tau^+\nu_\tau$ via the decay of $\tau^+ \to \mu^+\nu_\mu\bar{\nu}_\tau$, by analyzing 7.33 fb^{-1} of e^+e^- collision data taken at the center-of-mass energies $\sqrt{s} = 4.128$ GeV, 4.157 GeV, 4.178 GeV, 4.189 GeV, 4.199 GeV, 4.209 GeV, 4.219 GeV, and 4.226 GeV [25–27] with the BESIII detector [28]. Following previous measurements, we have not corrected the BF of $D_s^+ \to \tau^+\nu_\tau$ by the effect of radiative photons since their uncertainties can be considered individually later, details of which are reviewed in "*Leptonic Decays of Charged Pseudoscalar Mesons*" by the Particle Data Group (PDG) [24]. Based on this measurement, we determine $f_{D_s^+} \times |V_{\rm cs}|$ with an improved accuracy, and test $\tau - \mu$ lepton flavor universality with $D_s^+ \to \ell^+\nu_\ell$ decays.

2 BESIII detector and Monte Carlo simulation

The BESIII detector [28] records symmetric e^+e^- collisions provided by the BEPCII storage ring [29] in the center-of-mass energy range from 2.00 to 4.95 GeV, with a peak luminosity of 1×10^{33} cm^{-2} s^{-1} achieved at $\sqrt{s} = 3.77$ GeV. BESIII has collected large data samples in this energy region [30]. The cylindrical core of the BESIII detector covers 93% of the full solid angle and consists of a helium-based multilayer drift chamber (MDC), a plastic scintillator time-of-flight system (TOF), and a CsI(Tl) electromagnetic calorimeter (EMC), which are all enclosed in a superconducting solenoidal magnet providing a 1.0 T magnetic field [31]. The solenoid is supported by an octagonal flux-return yoke with modules of resistive plate muon counters (MUC) interleaved with steel. The charged-particle momentum resolution at 1 GeV/c is 0.5%, and specific ionization energy loss dE/dx resolution is 6% for electrons from Bhabha scattering. The EMC measures photon energies with a resolution of 2.5% (5%) at 1 GeV in the barrel (end-cap) region. The time resolution in the TOF barrel region is 68 ps. The end-cap TOF system was upgraded in 2015 using multi-gap resistive plate chamber technology, providing a time resolution of 60 ps [32–34]. Approximately 83% of the data used here was collected after this upgrade.

JHEP09(2023)124

Simulated data samples, namely inclusive MC samples, produced with a GEANT4-based [35] Monte Carlo (MC) package, which includes the geometric description of the BESIII detector and the detector response, are used to determine detection efficiencies and to estimate backgrounds. The simulation models the beam-energy spread and initial-state radiation (ISR) in the e^+e^- annihilations with the generator KKMC [36, 37]. In the simulation, the production of open-charm processes directly produced via e^+e^- annihilations are modeled with the generator CONEXC [38], and their subsequent decays are modeled by EVTGEN [39, 40] with known BFs from the Particle Data Group [24]. The ISR production of vector charmonium (-like) states and the continuum processes are incorporated in KKMC [36, 37]. The remaining unknown charmonium decays are modeled with LUNDCHARM [41, 42]. Final-state radiation from charged final-state particles is incorporated using the PHOTOS package [43]. The input cross section line shape of $e^+e^- \to D_s^{*\pm}D_s^{\mp}$ is based on the cross section measurement in the energy range from threshold to 4.7 GeV.

3 Analysis method

In e^+e^- collisions with data taken at the center-of-mass energies between 4.128 and 4.226 GeV, the $D_s^{\pm}$ mesons are produced mainly via the $e^+e^- \to D_s^{*\pm}D_s^{\mp} \to \gamma(\pi^0)D_s^+D_s^-$ process. For our analysis we adopt the double-tag (DT) method pioneered by the MARK III collaboration [44]. The D_s^- meson, when fully reconstructed via any hadronic decay mode, is referred to as the single-tag (ST) D_s^- meson. Events in which the transition $\gamma(\pi^0)$ from the D_s^{*+} meson and the leptonic decay of $D_s^+ \to \tau^+\nu_\tau$ are reconstructed, in addition to the ST D_s^- meson, are denoted as DT events. The BF of $D_s^+ \to \tau^+\nu_\tau$ is determined by

$$\mathcal{B}^j_{D_s^+\to\tau^+\nu_\tau} = \frac{N^j_{\rm DT}/\epsilon^j_{\rm DT}}{\mathcal{B}_{\tau^+\to\mu^+\nu_\mu\bar{\nu}_\tau} \cdot N^j_{\rm ST}/\epsilon^j_{\rm ST}}, \tag{3.1}$$

where $N^j_{\rm DT}$ and $N^j_{\rm ST}$ are the yields of the DT events and ST D_s^- mesons in data, respectively; and $\epsilon^j_{\rm DT}$ and $\epsilon^j_{\rm ST}$ are the efficiencies of the DT events and ST D_s^- mesons estimated with MC simulation, respectively. Here, $\epsilon^j_{\rm DT}$, which includes the efficiency of simultaneously finding the tag side, the transition $\gamma(\pi^0)$ and $D_s^+ \to \tau^+\nu_\tau$ as well as the BF of $D_s^{*+} \to \gamma(\pi^0)D_s^+$, $\mathcal{B}_{\tau^+\to\mu^+\nu_\mu\bar{\nu}_\tau}$ is the BF of $\tau^+ \to \mu^+\nu_\mu\bar{\nu}_\tau$ and j denotes the ST mode. The weighted mean method [45] is utilized to calculate the final BF, taking into account the statistical and tag mode dependent uncertainty as discussed later.

4 Single-tag candidates

To reconstruct ST D_s^- candidates, we use the fourteen hadronic decay modes $D_s^- \to K^+K^-\pi^-$, $K^+K^-\pi^-\pi^0$, $K^0_SK^-$, $K^0_SK^-\pi^0$, $K^0_SK^0_S\pi^-$, $K^0_SK^+\pi^-\pi^-$, $K^0_SK^-\pi^+\pi^-$, $\pi^+\pi^-\pi^-$, $\eta_{\gamma\gamma}\pi^-$, $\eta_{\pi^0\pi^+\pi^-}\pi^-$, $\eta'_{\eta_{\gamma\gamma}\pi^+\pi^-}\pi^-$, $\eta'_{\gamma\rho^0}\pi^-$, $\eta_{\gamma\gamma}\rho^-$, and $\eta_{\pi^+\pi^-\pi^0}\rho^-$. Throughout this paper, ρ denotes $\rho(770)$ and the subscripts of $\eta^{(\prime)}$ denote individual decay modes adopted for the $\eta^{(\prime)}$ reconstruction.

In selecting $K^{\pm}$, $\pi^{\pm}$, K^0_S, γ, π^0, and η candidates, we use the same selection criteria as those adopted in our previous studies [17, 46, 49]. For each good charged track, the polar angle (θ) with respect to the beam direction is required to be within the MDC acceptance $|\cos\theta| < 0.93$, where θ is defined with respect to the z axis, which is the symmetry axis of the MDC. The distance of its closest approach relative to the interaction point is required to be within 10.0 cm along the beam direction ($|V_z|$) and within 1.0 cm in the plane transverse to the beam direction ($|V_{xy}|$). Particle identification (PID) for good charged tracks combines the measurements of the $\mathrm{d}E/\mathrm{d}x$ in the MDC and the flight time in the TOF to form probabilities $\mathcal{L}(h)(h = K, \pi)$ for each hadron (h) hypothesis. The charged tracks are assigned as kaons or pions if their probabilities satisfy $\mathcal{L}(K) > \mathcal{L}(\pi)$ and $\mathcal{L}(\pi) > L(K)$, respectively.

The K_S^0 candidates are reconstructed via $K_S^0 \to \pi^+\pi^-$ decays. The two charged pions are required to satisfy $|V_z| < 20$ cm and $|\cos\theta| < 0.93$. They are assumed to be $\pi^+\pi^-$ without PID requirements and their invariant mass is required to be within $(0.486, 0.510)\,\mathrm{GeV}/c^2$. The distance from the K_S^0 decay vertex to the interaction point is required to be greater than twice the vertex resolution.

Photon candidates are selected by using the information measured by the EMC and are required to satisfy the following criteria. The energy of each shower in the barrel (end-cap) region of the EMC [28] is required to be greater than 25 (50) MeV. To suppress backgrounds associated with charged tracks, the angle between the shower position and the closest intersection point of any charged track with the EMC inner surface, projected from the interaction point, must be greater than 10 degrees. To suppress electronic noise and energy deposits unrelated to the event of interest, any candidate shower is required to start within [0, 700] ns from the event start time.

The π^0 and $\eta_{\gamma\gamma}$ candidates are formed from $\gamma\gamma$ pairs with invariant masses lying in the mass intervals (0.115, 0.150) and $(0.50, 0.57)\,\mathrm{GeV}/c^2$, respectively. To improve momentum resolution, each selected $\gamma\gamma$ pair is subjected to a kinematic fit that constrains their invariant mass to the known π^0 or η mass [24]. In order to form $\rho^{+(0)}$, $\eta_{\pi^0\pi^+\pi^-}$, $\eta'_{\eta\pi^+\pi^-}$, and $\eta'_{\gamma\rho^0}$ candidates, the invariant masses of the $\pi^+\pi^{0(-)}$, $\pi^0\pi^+\pi^-$, $\eta\pi^+\pi^-$, and $\gamma\rho^0$ combinations are required to lie within the mass intervals of $(0.57, 0.97)\,\mathrm{GeV}/c^2$, $(0.53, 0.57)\,\mathrm{GeV}/c^2$, $(0.946, 0.970)\,\mathrm{GeV}/c^2$ and $(0.940, 0.976)\,\mathrm{GeV}/c^2$, respectively. In addition, the energy of the photon from the $\eta'_{\gamma\rho^0}$ decay is required to be greater than 0.1 GeV.

Soft pions from D^{*+} decays are suppressed by requiring the momentum of any pion which is not from K_S^0, η, or η' to be greater than $0.1\,\mathrm{GeV}/c$. In order to reject the peaking background from $D_s^- \to K_S^0\pi^-$ decays in the selection of $D_s^- \to \pi^+\pi^-\pi^-$ STs, the invariant mass of any $\pi^+\pi^-$ combination is required to lie outside the mass window of $(0.468, 0.528)\,\mathrm{GeV}/c^2$.

The backgrounds from non-$D_s^\pm D_s^{*\mp}$ processes are suppressed by using the beam-constrained mass of the ST D_s^- candidate defined as

$$M_{\mathrm{BC}} \equiv \sqrt{E_{\mathrm{beam}}^2 - |\vec{p}_{\mathrm{ST}}|^2}, \tag{4.1}$$

where E_{beam} is the beam energy ($\sqrt{s}/2$) and $\vec{p}_{\mathrm{ST}}$ is the momentum of the ST D_s^- candidate in the e^+e^- rest frame. Figure 1 shows the M_{BC} distribution of the ST candidates at 4.178 GeV. The M_{BC} value is required to be within $(2.010, 2.061 + i \times 0.003)\,\mathrm{GeV}/c^2$, where

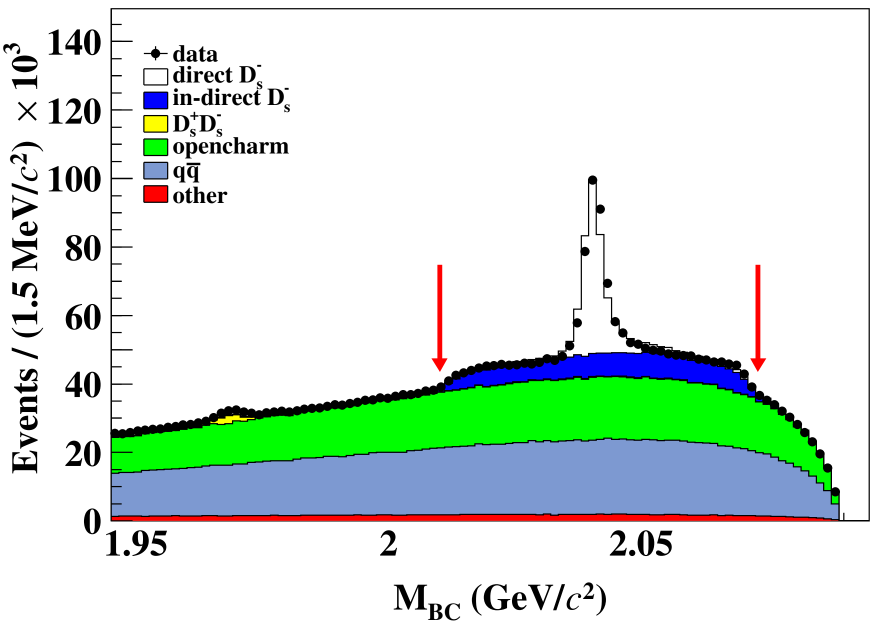

Figure 1. The $M_{\rm BC}$ distributions of the ST D_s^- candidates in data and inclusive MC samples at 4.178 GeV. The candidates between the two red arrows are retained for further analysis.

i takes the value 0, 3, 4, 5, 6, 7, 8, 9 for the energy points 4.128, 4.157, 4.178, 4.189, 4.199, 4.209, 4.219, 4.226, respectively. This requirement retains most of the D_s^- and D_s^+ mesons from $e^+e^- \to D_s^{*\mp}D_s^{\pm}$ production.

If there are multiple candidates present per tag mode per charge, only the one with the D_s^- recoil mass

$$M_{\rm rec} \equiv \sqrt{\left(\sqrt{s} - \sqrt{|\vec{p}_{\rm ST}|^2 + m^2_{D_s^-}}\right)^2 - |\vec{p}_{\rm ST}|^2} \tag{4.2}$$

closest to the D_s^{*+} nominal mass [24] is kept for further analysis.

The distributions of the invariant masses ($M_{\rm ST}$) of the accepted ST candidates from data for each tag mode are shown in figure 2. The yields of ST D_s^- mesons reconstructed in each tag mode are determined from fits to their individual $M_{\rm ST}$ distributions. In the fits, the signal is described by the simulated shape convolved with a Gaussian function that represents the resolution difference between data and simulation. In the fit to the $D_s^- \to K_S^0K^-$ tag mode, the shape of the peaking background $D^- \to K_S^0\pi^-$ is modeled by the simulated shape convolved with the same Gaussian resolution function as used for the signal shape and its size is left free. The fraction of the $D^- \to K_S^0\pi^-$ over $D_s^- \to K_S^0K^-$ yields is about 2.0%. The combinatorial background is described by a first to third order Chebychev function, which is validated by analyzing the inclusive MC sample. Figure 2 shows the fit results for the data sample at $\sqrt{s} = 4.178$ GeV. In each sub-figure, the red arrows show the chosen $M_{\rm ST}$ signal regions. The candidates located in these signal regions are retained for further analysis. Based on simulation, the $e^+e^- \to (\gamma_{\rm ISR})D_s^+D_s^-$ process is found to contribute about (0.7–1.1)% in the fitted number of ST D_s^- mesons for

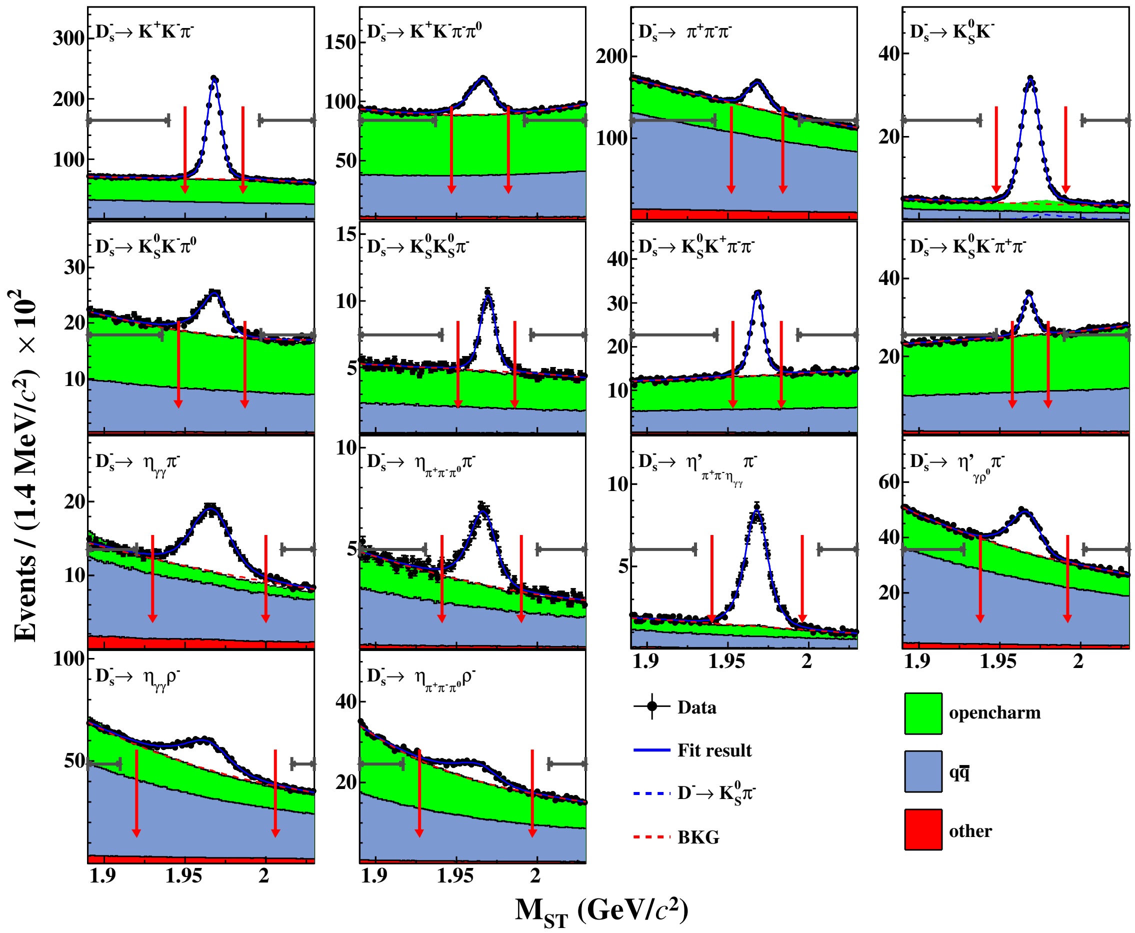

Figure 2. The fits to the $M_{\rm ST}$ distributions of the surviving ST D_s^- candidates for each tag mode. The points with error bars denote the data sample at $\sqrt{s} = 4.178\,\text{GeV}$. The blue solid curves represent the best fit results. The red dashed curves represent the fitted backgrounds. For the $D_s^- \to K_S^0K^-$ tag mode, the blue dotted curve is the peaking background from $D^- \to K_S^0\pi^-$. In each figure, the range within the two arrows indicate the chosen $M_{\rm ST}$ signal regions and the brown line segments indicate the sideband regions.

each tag mode. The reported yields have this contribution subtracted. The efficiencies of reconstructing ST D_s^- mesons ($N_{\rm ST}$) are estimated by analyzing the inclusive MC sample in the same way as real data.

The second and third columns of table 2 summarize the yields of ST D_s^- mesons ($N_{\rm ST}$) for each tag mode obtained in data and the corresponding detection efficiencies ($\epsilon_{\rm ST}$), respectively. In this table, the $N_{\rm ST}$ quantities are obtained by summing over all energy points, and the $\epsilon_{\rm ST}$ quantities are obtained by weighting the corresponding yields of ST D_s^- mesons in data at each energy points.

5 Double-tag candidates

The $D_s^+ \to \tau^+\nu_\tau$ candidates are selected in the system recoiling against the ST D_s^- mesons via the decay of $\tau^+ \to \mu^+\nu_\mu\bar{\nu}_\tau$ by using the residual neutral showers and charged tracks

JHEP09(2023)124

$\lvert\cos\theta_\mu\rvert$	p_μ (GeV/c)	d_μ (cm)
	$(0.50, 0.61)$	> 3.0
	$(0.61, 0.75)$	$> 100.0 \times p_\mu - 58.0$
$(0.0, 0.2)$	$(0.75, 0.88)$	> 17.0
	$(0.88, 1.04)$	$> 100.0 \times p_\mu - 71.0$
	$(1.04, 1.20)$	> 33.0
	$(0.50, 0.64)$	> 3.0
	$(0.64, 0.78)$	$> 100.0 \times p_\mu - 61.0$
$(0.2, 0.4)$	$(0.78, 0.91)$	> 17.0
	$(0.91, 1.07)$	$> 100.0 \times p_\mu - 74.0$
	$(1.07, 1.20)$	> 33.0
	$(0.50, 0.67)$	> 3.0
	$(0.67, 0.81)$	$> 100.0 \times p_\mu - 64.0$
$(0.4, 0.6)$	$(0.81, 0.94)$	> 17.0
	$(0.94, 1.10)$	$> 100.0 \times p_\mu - 77.0$
	$(1.10, 1.20)$	> 33.0
$(0.6, 0.8)$		> 9.0
$(0.8, 0.93)$		> 9.0

Table 1. Identification criteria for muon candidates.

which have not been used in the ST selection. As the detection efficiencies and background levels do not vary greatly with $\sqrt{s}$, the analysis combines the samples over all the energy points.

Excluding the daughter particles originating from the tag side, only one good charged track is allowed in each DT candidate and its charge must be opposite to that of the tag-side decay. The deposited energy of muon candidates in the EMC is required to be within $(0.0, 0.3)$ GeV. To separate muons from hadrons, the muon candidates must have momenta greater than $0.5\,\mathrm{GeV}/c$, and fulfill requirements on the muon travelling length in the MUC (d_μ) with dependence of momentum (p_μ) and flight direction ($\cos\theta_\mu$) in the MUC [17] as shown in table 1 and figure 3 based on the control sample of $e^+e^- \to \gamma\mu^+\mu^-$.

To select the $D_s^+ \to \tau^+\nu_\tau$ signals and the transition $\gamma(\pi^0)$ from D_s^{*+}, we define two kinematic variables: the energy difference

$$\Delta E \equiv \sqrt{s} - E_{\mathrm{ST}} - E_{\mathrm{miss}} - E_{\gamma(\pi^0)}, \tag{5.1}$$

where E_{miss} is defined as $\sqrt{|\vec{p}_{\mathrm{miss}}|^2 + m^2_{D_s^+}}$ with $\vec{p}_{\mathrm{miss}} \equiv -\vec{p}_{\mathrm{ST}} - \vec{p}_{\gamma(\pi^0)}$, and the missing mass squared of the neutrinos

$$M^2_{3\nu} \equiv \left(\sqrt{s} - \Sigma_k E_k\right)^2 - |\Sigma_k \vec{p}_k|^2, \tag{5.2}$$

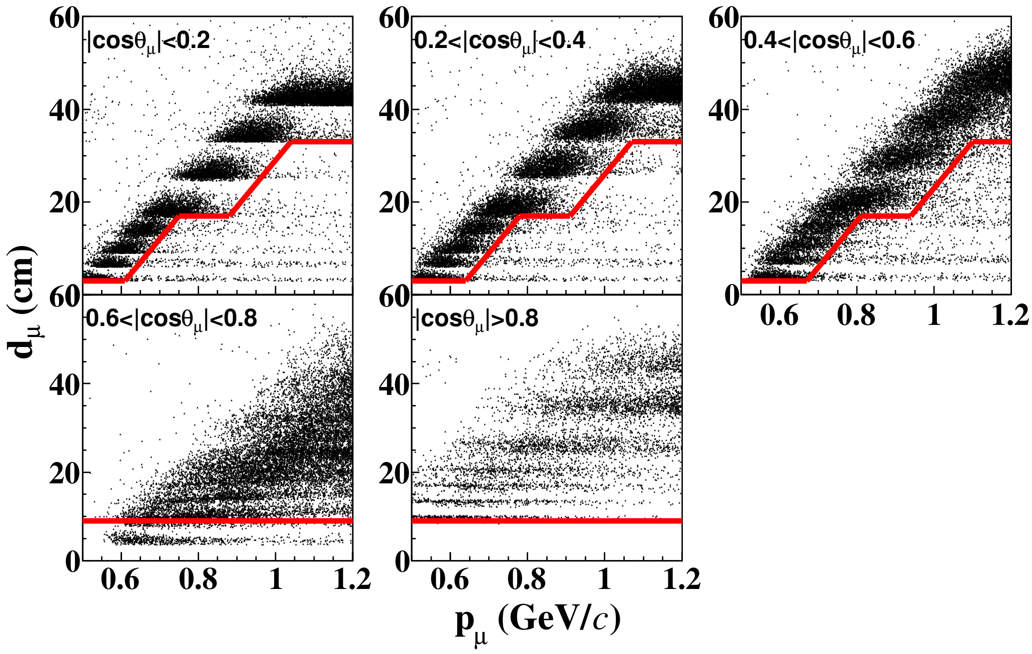

Figure 3. The distributions of d_μ vs. p_μ in different $|\cos\theta_\mu|$ regions of $e^+e^- \to \gamma\mu^+\mu^-$ candidates in data. The regions above the red line are retained for further analysis.

in which E_k and $\vec{p}_k$ are the energy and momentum of ST D_s^-, transition $\gamma(\pi^0)$, or μ^+, respectively. All γ and π^0 candidates that have not been used in tag selection are looped over. If there are multiple γ or π^0 combinations satisfying the selection criteria, we choose the one leading to the minimum $|\Delta E|$.

To suppress the backgrounds from $D_s^+ \to \mu^+\nu_\mu$ and $D_s^+ \to \eta\pi^+$ decays, which peak in the $M_{3\nu}^2$ distribution around 0 and $0.3\,\mathrm{GeV}^2/c^4$, respectively, the value of $M_{3\nu}^2$ is required to be within $(0.5, 2.0)\,\mathrm{GeV}^2/c^4$ as shown in figure 4.

6 Branching fraction determination

Following refs. [13, 21, 50], we discriminate signal from background by using the variable $E_{\mathrm{extra}\,\gamma}^{\mathrm{tot}}$. It is defined as the total energy of the good isolated EMC showers which have not been used in tag selection. The distributions of $E_{\mathrm{extra}\,\gamma}^{\mathrm{tot}}$ of the accepted DT candidates in data are shown in figure 5.

Study of the inclusive MC sample shows that the background events can be divided into three categories: BKGI, BKGII, and BKGIII. The BKGI component corresponds to events with an incorrectly reconstructed ST D_s^-. The BKGII component corresponds to events with a correctly reconstructed ST D_s^- and $D_s^+ \to K_L^0\mu^+\nu_\mu$, in which the K_L^0 meson passes through the detector without undergoing decay or significant interaction. The BKGIII component consists of events with a correctly reconstructed ST D_s^- and a D_s^+ decaying to any other background final state apart from $K_L^0\mu^+\nu_\mu$,

The DT signal yield is extracted by analyzing the $E_{\mathrm{extra}\,\gamma}^{\mathrm{tot}}$ distribution as shown in figure 5. To minimize the effect of the imperfect signal shape, we adopt an extrapolation

JHEP09(2023)124

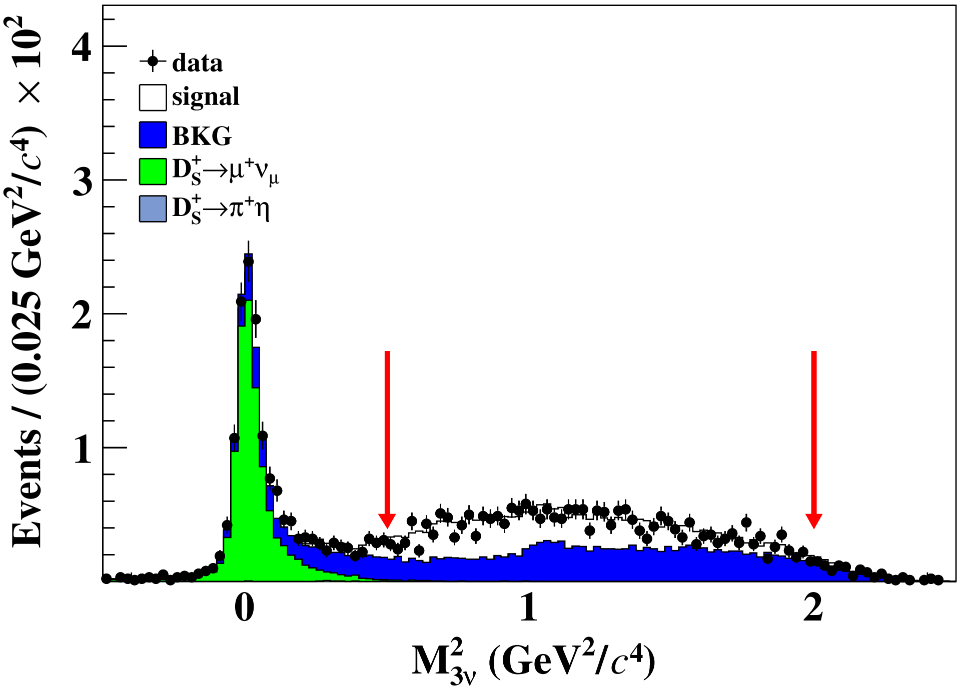

Figure 4. The $M^2_{3\nu}$ distributions of accepted candidates in data and inclusive MC samples with the $E^{\rm tot}_{{\rm extra}\ \gamma}$ <0.4 GeV requirement. Candidates with $M^2_{3\nu}$ within the two red arrows are retained for further analysis.

technique following refs. [13, 21, 50]. A bin maximum likelihood fit is performed on the events with $E^{\rm tot}_{{\rm extra}\,\gamma} > 0.6$ GeV, where the signal is negligible, and the sizes and shapes of BKGI and BKGII are fixed. The signal DT yield is obtained by subtracting the yields of BKGI, BKGII, and BKGIII from the yield of all events ($N^j_{\rm tot}$) in the $E^{\rm tot}_{{\rm extra}\gamma}$ signal region. In the D^*_s rest frame, the transition photon has a monochromatic energy of 139 MeV. When evaluated in the laboratory rest frame, the D^*_s momentum causes a smearing of $\pm$15 MeV on the photon energy. After further considering the resolution effect, we define $E^{\rm tot}_{{\rm extra}\gamma} <$ 0.4 GeV as the signal region. Details of BKGI, BKGII, and BKGIII are given below.

The shape of the BKGI component is derived using the data DT events situated in the corresponding $M_{\rm ST}$ sideband regions. The $M_{\rm ST}$ sideband regions are indicated inside the brown line segments in figure 2. For tag modes with neutrals, the remaining contamination from signal in sideband regions is subtracted. The size of this component is fixed at $f^j_1 \cdot N^{{\rm I}\,j}_{\rm Class}$, where f^j_1 is the sideband scale factor, defined as the ratio of the numbers of background events in the $M_{\rm ST}$ sideband and signal ranges. The f^j_1 value is obtained by fitting the $M_{\rm ST}$ distribution from the inclusive MC sample after imposing the DT requirements. $N^{{\rm I}\,j}_{\rm Class}$ is obtained by counting events in the $E^{\rm tot}_{{\rm extra}\,\gamma}$ signal region in data.

The shape of the BKGII component is modeled by the simulated events corrected by a 2D data-MC difference for the K^0_L detector response. The correction factors are obtained by using a control sample of $D^0 \to K^0_L\pi^+\pi^-$ decays from 2.93 fb^{-1} of e^+e^- collision data collected at $\sqrt{s} = 3.773$ GeV [51, 52]. The yield of this component is fixed at $N^{{\rm II}\,j}_{\rm Class}$, which is

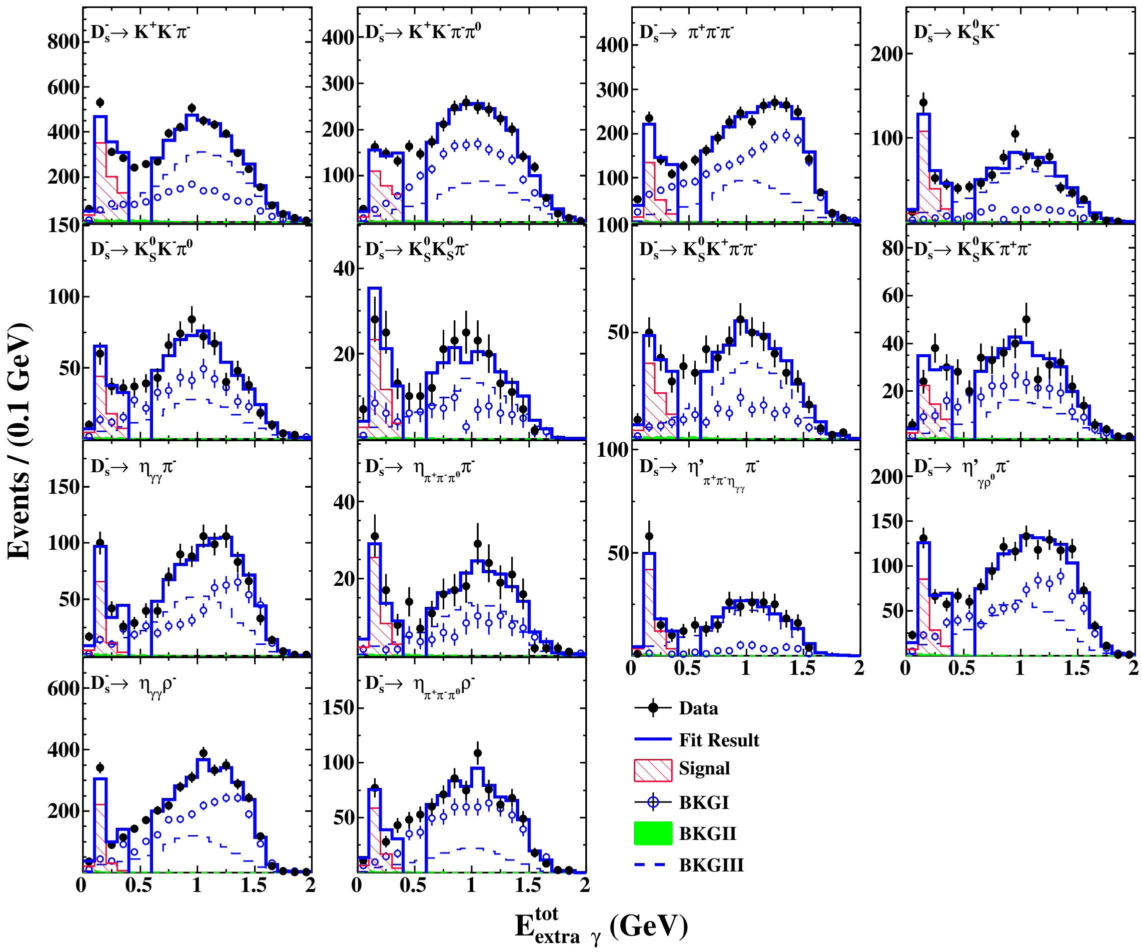

Figure 5. The distributions of $E^{\rm tot}_{{\rm extra}\,\gamma}$ of the DT candidates for $D_s^+ \to \tau^+\nu_\tau$ with $\tau^+ \to \mu^+\nu_\mu\bar{\nu}_\tau$. Black points with error bars are the combined data sample. Solid blue histograms denote the resutlts. Filled pink shadows, open circles with error bars, filled green histograms, and dashed blue histograms are Signal, BKGI, BKGII, and BKGIII, respectively.

calculated by taking the probability not to reconstruct the K^0_L meson from MC simulation and assuming the BF of $D_s^+ \to K^0\mu^+\nu_\mu$ decays to be the same as the corresponding decay mode involving electrons [24].

The shape of the BKGIII component is estimated from the inclusive MC sample. The MC simulation shows that the leading six D_s^+ non-peaking background components are $D_s^+ \to \eta\mu^+\nu_\mu$ (36.0%), $D_s^+ \to \eta\pi^+\pi^0$ (11.4%), $D_s^+ \to \pi^+\pi^0\nu_\tau\bar{\nu_\tau}$ (2.5%), $D_s^+ \to \phi\pi^+$ (2.5%), $D_s^+ \to \eta'\pi^+$ (2.5%), and $D_s^+ \to \phi\mu^+\nu_\mu$ (2.0%), where the numbers shown in parentheses are their proportional contribution to the total BKGIII in the full $E^{\rm tot}_{{\rm extra}\,\gamma}$ region. The yield of this component is represented by $f_2^j \cdot N^{{\rm III}\ j}_{\rm Class}$, where f_2^j is the extrapolation factor, defined as the ratio of the numbers of BKGIII events between $E^{\rm tot}_{{\rm extra}\,\gamma} < 0.4\,{\rm GeV}$ and $E^{\rm tot}_{{\rm extra}\,\gamma} > 0.6\,{\rm GeV}$ derived from the inclusive MC sample. The $N^{{\rm III}\ j}_{\rm Class}$ is obtained from the fit with $E^{\rm tot}_{{\rm extra}\,\gamma} > 0.6\,{\rm GeV}$.

Finally, the signal DT yield in data is obtained by

$$N_{\rm DT}^{j} = N_{\rm tot}^{j} - f_1^j \cdot N_{\rm Class}^{\rm I\ j} - N_{\rm Class}^{\rm II\ j} - f_2^j \cdot N_{\rm Class}^{\rm III\ j}. \tag{6.1}$$

The efficiencies of detecting DT events ($\epsilon_{\rm DT}^{j}$) are estimated by using the signal MC samples of $e^+e^- \to D_s^{\mp}D_s^{*\pm}$ with the D_s^- meson decaying to the tag mode and $D_s^+ \to \tau^+\nu_\tau$ with $\tau^+ \to \mu^+\nu_\mu\bar{\nu}_\tau$. All numbers discussed above are summarized in table 2. For each tag mode, inserting the individual values of $N_{\rm ST}^{j}$, $\epsilon_{\rm ST}^{j}$, $N_{\rm DT}^{j}$, and $\epsilon_{\rm DT}^{j}$ in eq. (3.1) gives the corresponding BF. The systematic uncertainties in the BF measurement are estimated in the next section. The obtained BFs are summarized in the last column of table 2.

7 Systematic uncertainties

Sources of the relative systematic uncertainties in the measurement of the BF of $D_s^+ \to \tau^+\nu_\tau$ are summarized in table 3 and discussed below. Note that the DT method means that most uncertainties due to the selection of ST D_s^- candidates cancel.

7.1 Tag-mode dependent systematic uncertainties

Several sources of potential systematic bias are associated with the tag mode, and are hence classified as tag-mode dependent.

The systematic uncertainties on the fitted yields of the ST D_s^- mesons are assessed by using alternative signal and background shapes. The alternative signal shapes are obtained by changing the baseline choices derived from inclusive MC sample to those from the signal MC sample. The alternative background shapes are obtained by varying the order of the nominal Chebychev function by ±1. For a given ST mode, the differences in the ratio of the yield of ST D_s^- mesons over the corresponding efficiency for all variations, and the background fluctuation of the fitted yield of ST D_s^- are re-weighted by the yields of ST D_s^- mesons in various data samples and are added in quadrature. An additional component to this uncertainty is statistical in nature, and accounts for the contribution of background fluctuations to the fitted yields of ST D_s^- mesons. The effects due to the signal shape, the background shape, and the background fluctuation are 0.08%, 0.12%, and 0.46%, respectively. The corresponding overall systematic uncertainty from all these sources is assigned to be 0.48%, which is the quadrature sum of these three terms.

The ST efficiencies obtained from the inclusive MC sample may differ from those estimated with the signal MC events generated with events containing the ST D_s^- and $D_s^+ \to \tau^+\nu_\tau$ decays, thereby causing possible tag bias. The size of this bias is estimated by measuring for each tag $\varepsilon_{\rm ST}^{D_s^+\to\tau^+\nu_\tau}$, the efficiency in the signal MC sample, and $\varepsilon_{\rm ST}^{{\rm inclusive}\, D_s^+}$, the efficiency in the inclusive MC sample, and multiplying $(\varepsilon_{\rm ST}^{D_s^+\to\tau^+\nu_\tau}/\varepsilon_{\rm ST}^{{\rm inclusive}\, D_s^+} - 1)$ by the estimated data-MC differences in the tracking and PID efficiencies without any correction, which are 1.0% for charged pions and kaons, and 2.0% for π^0, $\eta(\gamma\gamma)$ and K_S^0 decays. The resulting numbers are weighted by the ST yields in each tag to yield an overall systematic uncertainty of 0.37%.

After weighting by the yields of ST D_s^- mesons in each data sample, the uncertainty from the limited MC sample sizes is assigned to be 0.29%.

j	$N^j_{\rm ST}$ ($\times 10^3$)	$\epsilon^j_{\rm ST}$ (%)	$\epsilon^j_{\rm DT}$ (%)	$N^j_{\rm tot}$	f^j_1	$N^{{\rm I}\ j}_{\rm Class}$	$N^{{\rm II}\ j}_{\rm Class}$	f^j_2	$N^{{\rm III}\ j}_{\rm Class}$	$N^j_{\rm DT}$	$\mathcal{B}^j_{D_s^+\to\tau^+\nu_\tau}$ (%)
1	280.7±0.9	40.87±0.01	12.62±0.06	1184.0±34.4	0.422±0.001	531.0±23.0	54.0±6.8	0.080±0.001	2413.2±65.1	713.9±36.1	$5.42 \pm 0.27 \pm 0.05 \pm 0.14$
2	86.3±1.3	11.83±0.01	4.61±0.04	472.0±21.7	0.396±0.001	337.7±18.4	18.4±2.5	0.086±0.001	700.7±52.1	259.3±23.4	$5.08 \pm 0.46 \pm 0.13 \pm 0.13$
3	72.7±1.4	51.86±0.03	16.80±0.16	536.0±23.2	0.355±0.001	671.0±25.9	15.8±1.9	0.094±0.002	706.1±52.2	215.6±25.4	$6.02 \pm 0.71 \pm 0.13 \pm 0.16$
4	62.2±0.4	47.37±0.03	14.96±0.16	251.0±15.8	0.672±0.009	27.0±5.2	13.3±1.7	0.093±0.002	490.1±26.6	173.7±16.4	$5.81 \pm 0.55 \pm 0.08 \pm 0.15$
5	23.0±0.6	17.00±0.03	6.66±0.11	143.0±12.0	0.508±0.003	82.5±9.1	6.0±0.7	0.102±0.003	205.0±27.5	74.1±13.1	$5.42 \pm 0.96 \pm 0.18 \pm 0.14$
6	10.4±0.2	22.51±0.05	7.71±0.19	73.0±8.5	0.403±0.004	48.0±6.9	2.3±0.3	0.102±0.005	97.1±13.4	41.4±9.1	$7.65 \pm 1.68 \pm 0.25 \pm 0.20$
7	29.6±0.3	20.98±0.03	7.14±0.11	124.0±11.1	0.336±0.002	62.0±7.9	6.2±0.8	0.089±0.003	272.2±21.2	72.6±11.6	$4.73 \pm 0.76 \pm 0.09 \pm 0.12$
8	15.3±0.4	18.23±0.03	6.26±0.14	98.0±9.9	0.231±0.001	157.0±12.5	3.3±0.4	0.088±0.004	121.9±19.4	47.6±10.5	$5.96 \pm 1.31 \pm 0.21 \pm 0.16$
9	39.6±0.8	48.31±0.04	16.86±0.21	185.0±13.6	1.256±0.012	40.0±6.3	9.8±1.1	0.106±0.003	376.3±34.8	85.2±16.2	$4.06 \pm 0.77 \pm 0.11 \pm 0.11$
10	11.7±0.3	23.31±0.05	8.49±0.20	56.0±7.5	0.604±0.009	7.8±2.8	2.9±0.3	0.094±0.004	100.4±15.0	39.0±7.8	$6.02 \pm 1.20 \pm 0.22 \pm 0.16$
11	19.7±0.2	25.17±0.04	8.82±0.16	84.0±9.2	0.848±0.019	2.0±1.4	4.8±0.5	0.106±0.004	158.3±15.0	60.7±9.4	$5.78 \pm 0.89 \pm 0.15 \pm 0.15$
12	50.1±1.0	32.46±0.03	11.35±0.13	277.0±16.6	0.743±0.003	115.5±10.7	12.1±1.5	0.102±0.002	455.8±39.1	132.4±18.9	$4.97 \pm 0.71 \pm 0.12 \pm 0.13$
13	80.1±2.3	19.92±0.01	8.70±0.07	581.0±24.1	2.315±0.012	79.4±8.9	26.7±3.4	0.112±0.002	814.3±80.4	279.6±33.0	$5.25 \pm 0.62 \pm 0.18 \pm 0.14$
14	22.2±1.4	9.15±0.01	4.11±0.06	159.0±12.6	1.272±0.008	37.7±6.1	7.4±0.9	0.111±0.003	156.9±36.4	86.3±15.4	$5.70 \pm 1.01 \pm 0.39 \pm 0.15$

Table 2. The fitted yields of ST D_s^- mesons in data ($N^j_{\rm ST}$); the efficiencies of detecting ST D_s^- mesons ($\epsilon^j_{\rm ST}$) and DT events ($\epsilon^j_{\rm DT}$) for each tag mode; the number of total DT events ($N^j_{\rm tot}$); the sideband scale factor of BKGI (f^j_1); the extrapolation factor of BKGIII (f^j_2); the BKGI yield within $E^{\rm tot}_{{\rm extra}\,\gamma} < 0.4\,{\rm GeV}$ ($N^{{\rm I}\ j}_{\rm Class}$); the BKGII yield within $E^{\rm tot}_{{\rm extra}\,\gamma} < 0.4\,{\rm GeV}$ ($N^{{\rm II}\ j}_{\rm Class}$); the BKGIII yield within $E^{\rm tot}_{{\rm extra}\,\gamma} > 0.4\,{\rm GeV}$ ($N^{{\rm III}\ j}_{\rm Class}$); and the net numbers of DT events ($N^j_{\rm DT}$). For the obtained $\mathcal{B}^j_{D_s^+\to\tau^+\nu_\tau}$, the first, second, and third uncertainties are the statistical, tag-mode dependent systematic and tag-mode independent systematic, respectively. The listed efficiencies do not include the BFs of the sub decays. The index j from 1 to 14 represents the tag modes $D_s^- \to K^+K^-\pi^-$, $D_s^- \to K^+K^-\pi^-\pi^0$, $D_s^- \to \pi^+\pi^-\pi^-$, $D_s^- \to K^0_SK^-$, $D_s^- \to K^0_SK^-\pi^0$, $D_s^- \to K^0_SK^0_S\pi^-$, $D_s^- \to K^0_SK^+\pi^-\pi^-$, $D_s^- \to K^0_SK^-\pi^+\pi^-$, $D_s^- \to \eta_{\gamma\gamma}\pi^-$, $D_s^- \to \eta_{\pi^+\pi^-\pi^0}\pi^-$, $D_s^- \to \eta\prime_{\pi^+\pi^-\eta}\pi^-$, $D_s^- \to \eta\prime_{\gamma\rho^0}\pi^-$, $D_s^- \to \eta_{\gamma\gamma}\rho^-_{\pi^-\pi^0}$, and $D_s^- \to \eta_{\pi^+\pi^-\pi^0}\rho^-_{\pi^-\pi^0}$, respectively. The $\epsilon^j_{\rm DT}/\epsilon^j_{\rm ST}$ varies within 46% for different tag modes; this is mainly due to the significantly different signal environments for some tag modes containing low momentum photon and pions in the signal and inclusive MC samples.

Source	Uncertainty (%)
ST yield	0.48
Tag bias	0.37
MC sample size	0.29
μ^+ tracking	0.18
μ^+ PID	0.33
$\gamma(\pi^0)$ reconstruction	1.00
$M^2_{3\nu}$ requirement	1.75
$N^{\rm charge}_{\rm extra}$ requirement	0.41
$E^{\rm tot}_{{\rm extra}\,\gamma}$ fit	1.56
$\mathcal{B}(\tau^+ \to \mu^+\nu_\mu\bar{\nu}_\tau)$	0.23
Total	2.70

Table 3. Systematic uncertainties in the BF measurement.

7.2 Tag-mode independent systematic uncertainties

Systematic uncertainties which do not depend on tag modes are classified as tag-mode independent.

The systematic uncertainties related to the μ^+ tracking and PID efficiencies are investigated by using a control sample of $e^+e^- \to \gamma\mu^+\mu^-$ decays. By considering the dependencies of the μ^+ efficiencies on the μ^+ momentum, polar angle, and different energy points, the difference of μ^+ tracking efficiencies between data and MC simulation is $(-0.32 \pm 0.18)\%$. After correcting the signal efficiencies to data, the associated systematic uncertainty is assigned to be 0.18%. The difference of the μ^+ PID efficiencies between data and MC simulation is found to be $-(11.86 \pm 0.33)\%$. A similar large difference in the μ^+ PID efficiency between data and simulation was observed for $D_s^+ \to \mu^+\nu_\mu$ events in previous analyses at BESIII and is understood to arise from imperfections in the simulation of the length of the muon traveling in the MUC [17]. After correcting the signal efficiencies to data, the uncertainty 0.33% is assigned as the corresponding systematic uncertainty.

The efficiency of the γ selection is studied by using a control sample of $J/\psi \to \pi^+\pi^-\pi^0$ decays [53], while the π^0 reconstruction efficiency is studied with a sample of $e^+e^- \to K^+K^-\pi^+\pi^-\pi^0$ events [54]. The systematic uncertainty of selecting the transition γ or π^0 is estimated to be 1.00%, accounting for the relative BFs of $D_s^{*+} \to \gamma D_s^+$ and $D_s^{*+} \to \pi^0 D_s^+$ [24].

The systematic uncertainty associated with the $M^2_{3\nu}$ requirement is assessed by re-performing the measurement with enlarging or shrinking this requirement by ± 1 or ± 2 bin sizes, resulting in 24 variations. Among all variations, the maximum change of BF, 1.75%, is taken as the corresponding systematic uncertainty.

The systematic uncertainty associated with the requirement of no extra charged tracks ($N^{\rm charge}_{\rm extra}$) is studied with the DT sample of $D_s^+ \to \pi^+\phi(\to K^+K^-)$ and $D_s^+ \to K^+K^0_S(\to$

JHEP09(2023)124

$\pi^+\pi^-$). The difference of the acceptance efficiencies between data and MC simulation, 0.41%, is taken as the systematic uncertainty.

The systematic uncertainty in the $E^{\rm tot}_{{\rm extra}\,\gamma}$ fit has contributions associated with the three classes of background. The systematic uncertainty arising from the BKGI is estimated by varying the sideband scale factor by $\pm 1\sigma$ and the corresponding change of 0.10% in the fitted signal yield is taken as the systematic uncertainty. The systematic uncertainty arising from the shape of BKGII is assessed by replacing the corrected shape of $E^{\rm tot}_{{\rm extra}\,\gamma}$ with the uncorrected one and is found to be negligible. We also change the level of BKGII background by varying the misidentification rate by $\pm 1\sigma$ and the BF of $D_s^+ \to K_L^0 \mu^+\nu_\mu$ within the measurement uncertainty of the $D_s^+ \to K_L^0 e^+\nu_e$ BF. The relative difference of the fitted signal yield, 1.39%, is assigned as the associated systematic uncertainty. The uncertainty due to the non-peaking shape of BKGIII is estimated by varying the f_2 by $\pm 1\sigma$ and the relative components of the leading six background modes [24], and is assigned to be 0.69%. After adding these contributions in quadrature, the uncertainty associated with the $E^{\rm tot}_{{\rm extra}\,\gamma}$ fit is assigned to be 1.56%.

The uncertainty on the BF of $\tau^+ \to \mu^+\nu_\tau\bar{\nu}_\tau$ contributes a systematic uncertainty of 0.23% [24].

7.3 Total systematic uncertainties

By adding the individual components in quarature, we determine the total tag-mode dependent and independent systematic uncertainties to be 0.67% and 2.62%, respectively, and the total relative systematic uncertainty to be 2.70%.

8 Results

The measured values $\mathcal{B}_{D_s^+\to\tau^+\nu_\tau}$ are listed in table 2 for each tag mode. Weighting each measurement by the inverse squares of the combined statistical and tag-mode dependent systematic uncertainties yields

$$\mathcal{B}_{D_s^+\to\tau^+\nu_\tau} = (5.37 \pm 0.17_{\rm stat} \pm 0.15_{\rm syst})\%.$$

Here, the first uncertainty is statistical, and the second is the quadrature sum of the tag-mode dependent and independent systematic uncertainties. Using this BF and the world average values of $G_{\rm F}$, m_μ, $m_{D_s^+}$, and $\tau_{D_s^+}$ [24] with $\Gamma_{D_s^+\to\tau^+\nu_\tau} = \mathcal{B}_{D_s^+\to\tau^+\nu_\tau}/\tau_{D_s^+}$, we determine the product of $f_{D_s^+}$ and $|V_{cs}|$ to be

$$f_{D_s^+}|V_{cs}| = (246.7 \pm 3.9_{\rm stat} \pm 3.6_{\rm syst})\,{\rm MeV},$$

where the systematic uncertainty is dominated by that of the measured BF (2.70%) and the lifetime of D_s^+ (0.8%). Making use of $|V_{cs}| = 0.97349 \pm 0.00016$ from the global fit in the SM [24, 55], we obtain

$$f_{D_s^+} = (253.4 \pm 4.0_{\rm stat} \pm 3.7_{\rm syst})\,{\rm MeV}.$$

JHEP09(2023)124

Alternatively, utilizing $f_{D_s^+} = (249.9 \pm 0.5)$ MeV from recent LQCD calculations [2–4, 7], we obtain

$$|V_{cs}| = 0.987 \pm 0.016_{\rm stat} \pm 0.014_{\rm syst}.$$

In the calculation of $|V_{cs}|$, one additional uncertainty (0.2%) for the input value of $f_{D_s^+}$ is included. In the determination of $f_{D_s^+}$, however, the uncertainty from the input value $|V_{cs}|$ has negligible effect. Our value $|V_{cs}|$ agrees with our previous results obtained via $D \to \bar{K}\ell^+\nu_\ell$ [56–59], $D_s^+ \to \mu^+\nu_\mu$ [17, 18], and $D_s^+ \to \eta^{(\prime)}\ell^+\nu_\ell$ decays [46–48].

9 Summary

By analyzing e^+e^- collision data collected with a total integrated luminosity of $7.33\,\mathrm{fb}^{-1}$ at the center-of-mass energies between 4.128 GeV and 4.226 GeV, we determine the BF of $D_s^+ \to \tau^+\nu_\tau$ via $\tau^+ \to \mu^+\nu_\mu\bar{\nu}_\tau$ to be $(5.37 \pm 0.17_{\rm stat} \pm 0.15_{\rm syst})\%$. This result is consistent with the previous measurements [24]. Using this BF and the world average values of $G_{\rm F}$, m_μ, $m_{D_s^+}$, and $\tau_{D_s^+}$ [24] with $\Gamma_{D_s^+\to\tau^+\nu_\tau} = \mathcal{B}_{D_s^+\to\tau^+\nu_\tau}/\tau_{D_s^+}$, we determine the product of $f_{D_s^+}$ and $|V_{cs}|$ to be $f_{D_s^+}|V_{cs}| = (246.7 \pm 3.9_{\rm stat} \pm 3.6_{\rm syst})$ MeV. Combining the BF measured in this work with the $|V_{cs}|$ given by refs. [24, 55], we obtain $f_{D_s^+} = (253.4 \pm 4.0_{\rm stat} \pm 3.7_{\rm syst})$ MeV. Conversely, combining this BF with the $f_{D_s^+}$ calculated by LQCD [2–4, 7], we determine $|V_{cs}| = 0.987 \pm 0.016_{\rm stat} \pm 0.014_{\rm syst}$. Combining with the BF of $D_s^+ \to \mu^+\nu_\mu$ [24], we obtain $\mathcal{R}_{\tau/\mu} = 9.89 \pm 0.50$, which is consistent with the expectation based on lepton flavor universality.

We determine an average [45] BF for $D_s^+ \to \tau^+\nu_\tau$ and the derived quantities that follow from this result, taking as input the BF measurement from the current study, and those BF measurements using the decays $\tau^+ \to \pi^+\pi^0\bar{\nu}_\tau$ [20], $\tau^+ \to e^+\nu_e\bar{\nu}_\tau$ [21] and $\tau^+ \to \pi^+\bar{\nu}_\tau$ [22]. The uncertainties from the ST yield, the π^+ tracking efficiency, the soft $\gamma(\pi^0)$ reconstruction, the best transition $\gamma(\pi^0)$ selection, the tag bias, $\tau_{D_s^+}$, $m_{D_s^+}$, m_τ and $|V_{cs}|$ are taken to be correlated between the measurements. We determine the average BF to be $\mathcal{B}(D_s^+ \to \tau^+\nu_\tau) = (5.33 \pm 0.07_{\rm stat} \pm 0.08_{\rm syst})\%$. From this result it follows $f_{D_s^+} = (252.4 \pm 1.7_{\rm stat} \pm 2.1_{\rm syst})$ MeV, $|V_{cs}| = 0.983 \pm 0.007_{\rm stat} \pm 0.008_{\rm syst}$, and $\mathcal{R}_{\tau/\mu} = 9.82 \pm 0.33$, again consistent with the expectation based on the assumption of lepton flavor universality. Figures 6, 7, and 8 show comparisons of our results for $\mathcal{B}(D_s^+ \to \tau^+\nu_\tau)$, $f_{D_s^+}$, and $|V_{cs}|$ with those of previous results.

Improved measurements of $\mathcal{B}(D_s^+ \to \tau^+\nu_\tau)$ are foreseen with the larger data sets that BESIII is expected to accumulate in the coming years [30].

Acknowledgments

The BESIII collaboration thanks the staff of BEPCII and the IHEP computing center for their strong support. This work is supported in part by National Key R&D Program of China under Contracts Nos. 2020YFA0406400, 2020YFA0406300; National Natural Science Foundation of China (NSFC) under Contracts Nos. 11875170, 12105076, 11635010, 11735014, 11835012, 11935015, 11935016, 11935018, 11961141012, 12022510, 12025502, 12035009, 12035013, 12061131003, 12192260, 12192261, 12192262, 12192263, 12192264, 12192265; the Chinese Academy of Sciences (CAS) Large-Scale Scientific Facility Program;

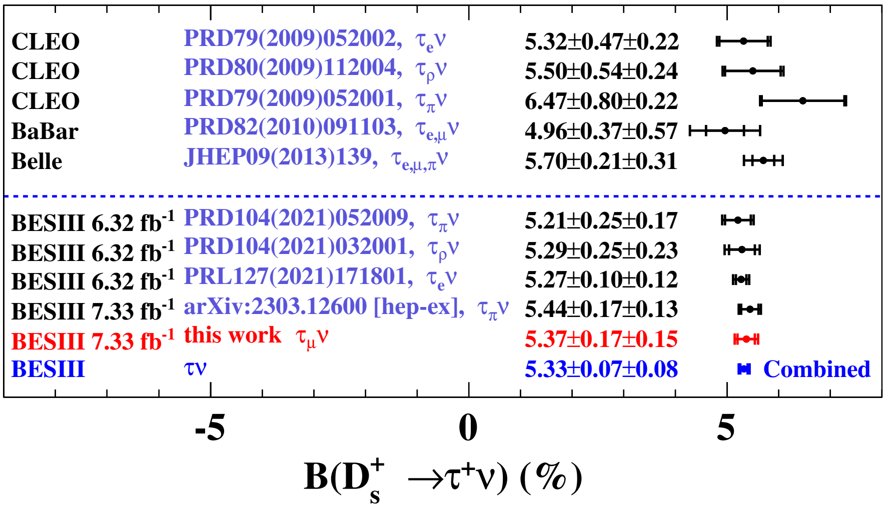

Figure 6. Comparison of the BFs measured in this work with previous measurements, where the inner error bar is the statistical uncertainty and the outer is the combined statistical and systematic uncertainty. The last line is the BESIII combined result which does not include the BESIII result in ref. [19].

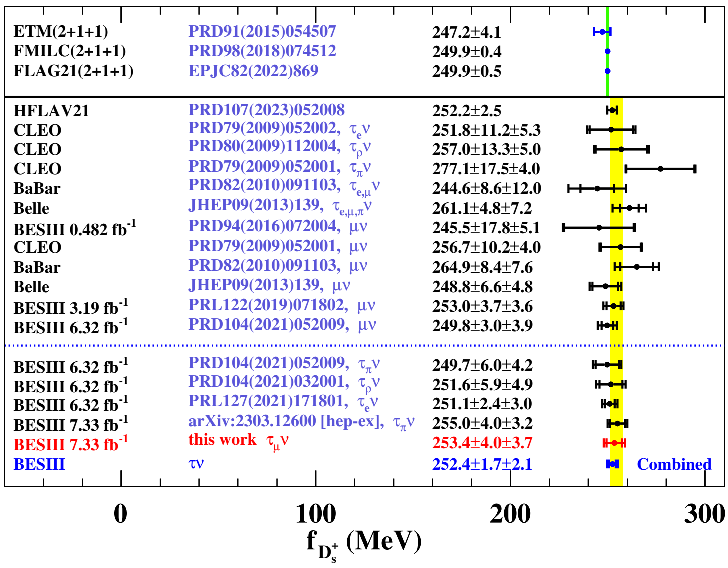

Figure 7. Comparison of $f_{D_s^+}$ values in this with previous work and LQCD calculations. For experimental results, the inner error bar is the statistical uncertainty and the outer is the combined statistical and systematic uncertainty. The green band denotes the FLAG average and the yellow one denotes the experimental average. The last line is the BESIII combined result which does not include the BESIII result in ref. [19].

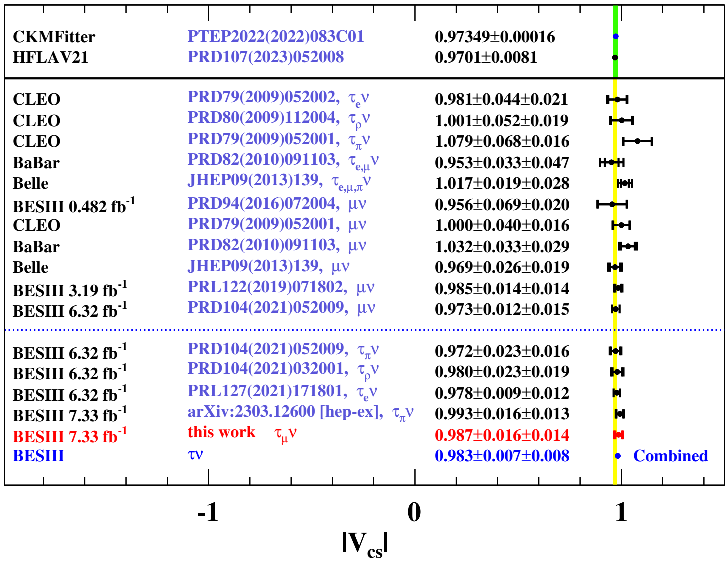

Figure 8. Comparison of $|V_{\rm cs}|$ values in this with previous work. For experimental results, the inner error bar is the statistical uncertainty and the outer is the combined statistical and systematic uncertainty. The green band denotes the CKM Fitter average and the yellow one denotes the experimental average. The last line is the BESIII combined result which does not include the BESIII result in ref. [19].

the CAS Center for Excellence in Particle Physics (CCEPP); Joint Large-Scale Scientific Facility Funds of the NSFC and CAS under Contract No. U1832207; CAS Key Research Program of Frontier Sciences under Contracts Nos. QYZDJ-SSW-SLH003, QYZDJ-SSW-SLH040; 100 Talents Program of CAS; The Institute of Nuclear and Particle Physics (INPAC) and Shanghai Key Laboratory for Particle Physics and Cosmology; ERC under Contract No. 758462; European Union's Horizon 2020 research and innovation programme under Marie Sklodowska-Curie grant agreement under Contract No. 894790; German Research Foundation DFG under Contracts Nos. 443159800, 455635585, Collaborative Research Center CRC 1044, FOR5327, GRK 2149; Istituto Nazionale di Fisica Nucleare, Italy; Ministry of Development of Turkey under Contract No. DPT2006K-120470; National Research Foundation of Korea under Contract No. NRF-2022R1A2C1092335; National Science and Technology fund; National Science Research and Innovation Fund (NSRF) via the Program Management Unit for Human Resources & Institutional Development, Research and Innovation under Contract No. B16F640076; Polish National Science Centre under Contract No. 2019/35/O/ST2/02907; Suranaree University of Technology (SUT), Thailand Science Research and Innovation (TSRI), and National Science Research and Innovation Fund (NSRF) under Contract No. 160355; The Royal Society, U.K. under Contract No. DH160214; The Swedish Research Council; U.S. Department of Energy under Contract No. DE-FG02-05ER41374.

References

[1] D. Silverman and H. Yao, *Relativistic Treatment of Light Quarks in D and B Mesons and W Exchange Weak Decays*, Phys. Rev. D **38** (1988) 214 [INSPIRE].

[2] A. Bazavov et al., *B- and D-meson leptonic decay constants from four-flavor lattice QCD*, Phys. Rev. D **98** (2018) 074512 [arXiv:1712.09262] [INSPIRE].

[3] Fermilab Lattice and MILC collaborations, *Charmed and Light Pseudoscalar Meson Decay Constants from Four-Flavor Lattice QCD with Physical Light Quarks*, Phys. Rev. D **90** (2014) 074509 [arXiv:1407.3772] [INSPIRE].

[4] N. Carrasco et al., *Leptonic decay constants f_K, f_D, and f_{D_s} with $N_f = 2+1+1$ twisted-mass lattice QCD*, Phys. Rev. D **91** (2015) 054507 [arXiv:1411.7908] [INSPIRE].

[5] P.A. Boyle, L. Del Debbio, A. Jüttner, A. Khamseh, F. Sanfilippo and J.T. Tsang, *The decay constants f_D and f_{D_s} in the continuum limit of $N_f = 2+1$ domain wall lattice QCD*, JHEP **12** (2017) 008 [arXiv:1701.02644] [INSPIRE].

[6] Y.-B. Yang et al., *Charm and strange quark masses and f_{D_s} from overlap fermions*, Phys. Rev. D **92** (2015) 034517 [arXiv:1410.3343] [INSPIRE].

[7] Flavour Lattice Averaging Group (FLAG) collaboration, *FLAG Review 2021*, Eur. Phys. J. C **82** (2022) 869 [arXiv:2111.09849] [INSPIRE].

[8] TWQCD collaboration, *Decay Constants of Pseudoscalar D-mesons in Lattice QCD with Domain-Wall Fermion*, Phys. Lett. B **736** (2014) 231 [arXiv:1404.3648] [INSPIRE].

[9] D. Becirevic, B. Blossier, A. Gerardin, A. Le Yaouanc and F. Sanfilippo, *On the significance of B-decays to radially excited D*, Nucl. Phys. B **872** (2013) 313 [arXiv:1301.7336] [INSPIRE].

[10] Z.-G. Wang, *Analysis of the masses and decay constants of the heavy-light mesons with QCD sum rules*, Eur. Phys. J. C **75** (2015) 427 [arXiv:1506.01993] [INSPIRE].

[11] CLEO collaboration, *Measurement of $\mathscr{B}(D_s^+ \to \ell^+\nu)$ and the Decay Constant $f_{D_s^+}$ From $600\,pb^{-1}$ of e^+e^- Annihilation Data Near $4170\,MeV$*, Phys. Rev. D **79** (2009) 052001 [arXiv:0901.1216] [INSPIRE].

[12] CLEO collaboration, *Measurement of the Pseudoscalar Decay Constant $f_{D_s^+}$ Using $D_s^+ \to \tau^+\nu_\tau$, $\tau^+ \to \rho^+\bar{\nu}_\tau$ Decays*, Phys. Rev. D **80** (2009) 112004 [arXiv:0910.3602] [INSPIRE].

[13] CLEO collaboration, *Improved Measurement of Absolute Branching Fraction of $D_s^+ \to \tau^+\nu_\tau$*, Phys. Rev. D **79** (2009) 052002 [arXiv:0901.1147] [INSPIRE].

[14] BaBar collaboration, *Measurement of the Absolute Branching Fractions for $D_s^- \to \ell^-\bar{\nu}_\ell$ and Extraction of the Decay Constant f_{D_s}*, Phys. Rev. D **82** (2010) 091103 [*Erratum ibid.* **91** (2015) 019901] [arXiv:1008.4080] [INSPIRE].

[15] ATLAS collaboration, *Searches for electroweak production of supersymmetric particles with compressed mass spectra in $\sqrt{s} = 13$ TeV pp collisions with the ATLAS detector*, Phys. Rev. D **101** (2020) 052005 [arXiv:1911.12606] [INSPIRE].

[16] BESIII collaboration, *Measurement of the $D_s^+ \to \ell^+\nu_\ell$ branching fractions and the decay constant $f_{D_s^+}$*, Phys. Rev. D **94** (2016) 072004 [arXiv:1608.06732] [INSPIRE].

[17] BESIII collaboration, *Determination of the pseudoscalar decay constant $f_{D_s^+}$ via $D_s^+ \to \mu^+\nu_\mu$*, Phys. Rev. Lett. **122** (2019) 071802 [arXiv:1811.10890] [INSPIRE].

[18] BESIII collaboration, *Improved measurement of the branching fraction of $D_s^+ \to \mu^+\nu_\mu$*, arXiv:2307.14585 [INSPIRE].

[19] BESIII collaboration, *Measurement of the absolute branching fractions for purely leptonic D_s^+ decays*, Phys. Rev. D **104** (2021) 052009 [arXiv:2102.11734] [INSPIRE].

[20] BESIII collaboration, *Measurement of the branching fraction of leptonic decay $D_s^+ \to \tau^+\nu_\tau$ via $\tau^+ \to \pi^+\pi^0\bar{\nu}_\tau$*, Phys. Rev. D **104** (2021) 032001 [arXiv:2105.07178] [INSPIRE].

[21] BESIII collaboration, *Measurement of the Absolute Branching Fraction of $D_s^+ \to \tau^+\nu_\tau$ via $\tau^+ \to e^+\nu_e\bar{\nu}_\tau$*, Phys. Rev. Lett. **127** (2021) 171801 [arXiv:2106.02218] [INSPIRE].

[22] BESIII collaboration, *Updated measurement of the branching fraction of $D_s^+ \to \tau^+\nu_\tau$ via $\tau^+ \to \pi^+\bar{\nu}_\tau$*, arXiv:2303.12600 [INSPIRE].

[23] H.-B. Li and X.-R. Lyu, *Study of the standard model with weak decays of charmed hadrons at BESIII*, Natl. Sci. Rev. **8** (2021) nwab181 [arXiv:2103.00908] [INSPIRE].

[24] Particle Data collaboration, *Review of Particle Physics*, Prog. Theor. Exp. Phys. **2022** (2022) 083C01 [INSPIRE].

[25] BESIII collaboration, *Measurement of the center-of-mass energies at BESIII via the di-muon process*, Chin. Phys. C **40** (2016) 063001 [arXiv:1510.08654] [INSPIRE].

[26] BESIII collaboration, *Precision measurement of the integrated luminosity of the data taken by BESIII at center of mass energies between* 3.810 *GeV and* 4.600 *GeV*, Chin. Phys. C **39** (2015) 093001 [arXiv:1503.03408] [INSPIRE].

[27] BESIII collaboration, *Measurement of integrated luminosities at BESIII for data samples at center-of-mass energies between* 4.0 *and* 4.6 *GeV*, Chin. Phys. C **46** (2022) 113002 [arXiv:2203.03133] [INSPIRE].

[28] BESIII collaboration, *Design and Construction of the BESIII Detector*, Nucl. Instrum. Meth. A **614** (2010) 345 [arXiv:0911.4960] [INSPIRE].

[29] C. Yu et al., *BEPCII Performance and Beam Dynamics Studies on Luminosity*, in proceedings of the *7th International Particle Accelerator Conference*, Busan, Republic of Korea, 8–13 May 2016 [DOI:10.18429/JACoW-IPAC2016-TUYA01] [INSPIRE].

[30] BESIII collaboration, *Future Physics Programme of BESIII*, Chin. Phys. C **44** (2020) 040001 [arXiv:1912.05983] [INSPIRE].

[31] K.-X. Huang et al., *Method for detector description transformation to Unity and application in BESIII*, Nucl. Sci. Tech. **33** (2022) 142 [arXiv:2206.10117] [INSPIRE].

[32] X. Li et al., *Study of MRPC technology for BESIII endcap-TOF upgrade*, Radiat. Detect. Technol. Meth. **1** (2017) 13.

[33] Y.-X. Guo et al., *The study of time calibration for upgraded end cap TOF of BESIII*, Radiat. Detect. Technol. Meth. **1** (2017) 15.

[34] P. Cao et al., *Design and construction of the new BESIII endcap Time-of-Flight system with MRPC Technology*, Nucl. Instrum. Meth. A **953** (2020) 163053 [INSPIRE].

[35] GEANT4 collaboration, *GEANT4 — a simulation toolkit*, Nucl. Instrum. Meth. A **506** (2003) 250 [INSPIRE].

[36] S. Jadach, B.F.L. Ward and Z. Was, *Coherent exclusive exponentiation for precision Monte Carlo calculations*, Phys. Rev. D **63** (2001) 113009 [hep-ph/0006359] [INSPIRE].

[37] S. Jadach, B.F.L. Ward and Z. Was, *The Precision Monte Carlo event generator KK for two fermion final states in e^+e^- collisions*, Comput. Phys. Commun. **130** (2000) 260 [hep-ph/9912214] [INSPIRE].

[38] R.-G. Ping, *An exclusive event generator for e^+e^- scan experiments*, Chin. Phys. C **38** (2014) 083001 [arXiv:1309.3932] [INSPIRE].

[39] D.J. Lange, *The EvtGen particle decay simulation package*, *Nucl. Instrum. Meth. A* **462** (2001) 152 [INSPIRE].

[40] R.-G. Ping, *Event generators at BESIII*, *Chin. Phys. C* **32** (2008) 599 [INSPIRE].

[41] J.C. Chen, G.S. Huang, X.R. Qi, D.H. Zhang and Y.S. Zhu, *Event generator for J/ψ and $\psi(2S)$ decay*, *Phys. Rev. D* **62** (2000) 034003 [INSPIRE].

[42] R.-L. Yang, R.-G. Ping and H. Chen, *Tuning and Validation of the Lundcharm Model with J/ψ Decays*, *Chin. Phys. Lett.* **31** (2014) 061301 [INSPIRE].

[43] E. Richter-Was, *QED bremsstrahlung in semileptonic B and leptonic tau decays*, *Phys. Lett. B* **303** (1993) 163 [INSPIRE].

[44] MARK-III collaboration, *Direct Measurements of Charmed d Meson Hadronic Branching Fractions*, *Phys. Rev. Lett.* **56** (1986) 2140 [INSPIRE].

[45] M. Schmelling, *Averaging correlated data*, *Phys. Scr.* **51** (1995) 676 [INSPIRE].

[46] BESIII collaboration, *Measurement of the Dynamics of the Decays $D_s^+ \to \eta^{(\prime)} e^+ \nu_e$*, *Phys. Rev. Lett.* **122** (2019) 121801 [arXiv:1901.02133] [INSPIRE].

[47] BESIII collaboration, *Precision Measurements of $D_s^+ \to \eta e^+ \nu_e$ and $D_s^+ \to \eta' e^+ \nu_e$*, arXiv:2306.05194 [INSPIRE].

[48] BESIII collaboration, *Observation of $D_s^+ \to \eta' \mu^+ \nu_\mu$ and Measurements of $D_s^+ \to \eta^{(\prime)} \mu^+ \nu_\mu$ Decay Dynamics*, arXiv:2307.12852 [INSPIRE].

[49] BESIII collaboration, *Search for the decay $D_s^+ \to \gamma e^+ \nu_e$*, *Phys. Rev. D* **99** (2019) 072002 [arXiv:1902.03351] [INSPIRE].

[50] CLEO collaboration, *Measurement of the absolute branching fraction of $D_s^+ \to \tau^+ \nu_\tau$ decay*, *Phys. Rev. Lett.* **100** (2008) 161801 [arXiv:0712.1175] [INSPIRE].

[51] BESIII collaboration, *Measurement of the integrated luminosities of the data taken by BESIII at $\sqrt{s} = 3.650$ and 3.773 GeV*, *Chin. Phys. C* **37** (2013) 123001 [arXiv:1307.2022] [INSPIRE].

[52] BESIII collaboration, *Measurement of the $e^+e^- \to \pi^+\pi^-$ cross section between 600 and 900 MeV using initial state radiation*, *Phys. Lett. B* **753** (2016) 629 [*Erratum ibid.* **812** (2021) 135982] [arXiv:1507.08188] [INSPIRE].

[53] BESIII collaboration, *Study of χ_{cJ} radiative decays into a vector meson*, *Phys. Rev. D* **83** (2011) 112005 [arXiv:1103.5564] [INSPIRE].

[54] BESIII collaboration, *Observation of the W-Annihilation Decay $D_s^+ \to \omega\pi^+$ and Evidence for $D_s^+ \to \omega K^+$*, *Phys. Rev. D* **99** (2019) 091101 [arXiv:1811.00392] [INSPIRE].

[55] CKMfitter Group, *CP violation and the CKM matrix: Assessing the impact of the asymmetric B factories*, *Eur. Phys. J. C* **41** (2005) 1 [hep-ph/0406184] [INSPIRE].

[56] BESIII collaboration, *Study of Dynamics of $D^0 \to K^- e^+ \nu_e$ and $D^0 \to \pi^- e^+ \nu_e$ Decays*, *Phys. Rev. D* **92** (2015) 072012 [arXiv:1508.07560] [INSPIRE].

[57] BESIII collaboration, *Analysis of $D^+ \to \bar{K}^0 e^+ \nu_e$ and $D^+ \to \pi^0 e^+ \nu_e$ semileptonic decays*, *Phys. Rev. D* **96** (2017) 012002 [arXiv:1703.09084] [INSPIRE].

[58] BESIII collaboration, *Study of decay dynamics and CP asymmetry in $D^+ \to K_L^0 e^+ \nu_e$ decay*, *Phys. Rev. D* **92** (2015) 112008 [arXiv:1510.00308] [INSPIRE].

[59] BESIII collaboration, *Study of the $D^0 \to K^- \mu^+ \nu_\mu$ dynamics and test of lepton flavor universality with $D^0 \to K^- \ell^+ \nu_\ell$ decays*, *Phys. Rev. Lett.* **122** (2019) 011804 [arXiv:1810.03127] [INSPIRE].

JHEP09(2023)124

The BESIII collaboration

M. Ablikim[1], M.N. Achasov[13,b], P. Adlarson[73], R. Aliberti[34], A. Amoroso[72A,72C], M.R. An[38], Q. An[69,56], Y. Bai[55], O. Bakina[35], I. Balossino[29A], Y. Ban[45,g], V. Batozskaya[1,43], K. Begzsuren[31], N. Berger[34], M. Bertani[28A], D. Bettoni[29A], F. Bianchi[72A,72C], E. Bianco[72A,72C], J. Bloms[66], A. Bortone[72A,72C], I. Boyko[35], R.A. Briere[5], A. Brueggemann[66], H. Cai[74], X. Cai[1,56], A. Calcaterra[28A], G.F. Cao[1,61], N. Cao[1,61], S.A. Cetin[60A], J.F. Chang[1,56], T.T. Chang[75], W.L. Chang[1,61], G.R. Che[42], G. Chelkov[35,a], C. Chen[42], Chao Chen[53], G. Chen[1], H.S. Chen[1,61], M.L. Chen[1,56,61], S.J. Chen[41], S.M. Chen[59], T. Chen[1,61], X.R. Chen[30,61], X.T. Chen[1,61], Y.B. Chen[1,56], Y.Q. Chen[33], Z.J. Chen[25,h], W.S. Cheng[72C], S.K. Choi[10], X. Chu[42], G. Cibinetto[29A], S.C. Coen[4], F. Cossio[72C], J.J. Cui[48], H.L. Dai[1,56], J.P. Dai[77], A. Dbeyssi[19], R.E. de Boer[4], D. Dedovich[35], Z.Y. Deng[1], A. Denig[34], I. Denysenko[35], M. Destefanis[72A,72C], F. De Mori[72A,72C], B. Ding[64,1], X.X. Ding[45,g], Y. Ding[39], Y. Ding[33], J. Dong[1,56], L.Y. Dong[1,61], M.Y. Dong[1,56,61], X. Dong[74], S.X. Du[79], Z.H. Duan[41], P. Egorov[35,a], Y.L. Fan[74], J. Fang[1,56], S.S. Fang[1,61], W.X. Fang[1], Y. Fang[1], R. Farinelli[29A], L. Fava[72B,72C], F. Feldbauer[4], G. Felici[28A], C.Q. Feng[69,56], J.H. Feng[57], K. Fischer[67], M. Fritsch[4], C. Fritzsch[66], C.D. Fu[1], Y.W. Fu[1], H. Gao[61], Y.N. Gao[45,g], Yang Gao[69,56], S. Garbolino[72C], I. Garzia[29A,29B], P.T. Ge[74], Z.W. Ge[41], C. Geng[57], E.M. Gersabeck[65], A. Gilman[67], K. Goetzen[14], L. Gong[39], W.X. Gong[1,56], W. Gradl[34], S. Gramigna[29A,29B], M. Greco[72A,72C], M.H. Gu[1,56], Y.T. Gu[16], C.Y. Guan[1,61], Z.L. Guan[22], A.Q. Guo[30,61], L.B. Guo[40], R.P. Guo[47], Y.P. Guo[12,f], A. Guskov[35,a], X.T. Hou[1,61], W.Y. Han[38], X.Q. Hao[20], F.A. Harris[63], K.K. He[53], K.L. He[1,61], F.H. Heinsius[4], C.H. Heinz[34], Y.K. Heng[1,56,61], C. Herold[58], T. Holtmann[4], P.C. Hong[12,f], G.Y. Hou[1,61], Y.R. Hou[61], Z.L. Hou[1], H.M. Hu[1,61], J.F. Hu[54,i], T. Hu[1,56,61], Y. Hu[1], G.S. Huang[69,56], K.X. Huang[57], L.Q. Huang[30,61], X.T. Huang[48], Y.P. Huang[1], T. Hussain[71], N. Hüsken[27,34], W. Imoehl[27], M. Irshad[69,56], J. Jackson[27], S. Jaeger[4], S. Janchiv[31], J.H. Jeong[10], Q. Ji[1], Q.P. Ji[20], X.B. Ji[1,61], X.L. Ji[1,56], Y.Y. Ji[48], Z.K. Jia[69,56], P.C. Jiang[45,g], S.S. Jiang[38], T.J. Jiang[17], X.S. Jiang[1,56,61], Y. Jiang[61], J.B. Jiao[48], Z. Jiao[23], S. Jin[41], Y. Jin[64], M.Q. Jing[1,61], T. Johansson[73], X. Kui[1], S. Kabana[32], N. Kalantar-Nayestanaki[62], X.L. Kang[9], X.S. Kang[39], R. Kappert[62], M. Kavatsyuk[62], B.C. Ke[79], A. Khoukaz[66], R. Kiuchi[1], R. Kliemt[14], L. Koch[36], O.B. Kolcu[60A], B. Kopf[4], M. Kuessner[4], A. Kupsc[43,73], W. Kühn[36], J.J. Lane[65], J.S. Lange[36], P. Larin[19], A. Lavania[26], L. Lavezzi[72A,72C], T.T. Lei[69,k], Z.H. Lei[69,56], H. Leithoff[34], M. Lellmann[34], T. Lenz[34], C. Li[46], C. Li[42], C.H. Li[38], Cheng Li[69,56], D.M. Li[79], F. Li[1,56], G. Li[1], H. Li[69,56], H.B. Li[1,61], H.J. Li[20], H.N. Li[54,i], Hui Li[42], J.R. Li[59], J.S. Li[57], J.W. Li[48], Ke Li[1], L.J. Li[1,61], L.K. Li[1], Lei Li[3], M.H. Li[42], P.R. Li[37,j,k], S.X. Li[12], T. Li[48], W.D. Li[1,61], W.G. Li[1], X.H. Li[69,56], X.L. Li[48], Xiaoyu Li[1,61], Y.G. Li[45,g], Z.J. Li[57], Z.X. Li[16], Z.Y. Li[57], C. Liang[41], H. Liang[69,56], H. Liang[33], H. Liang[1,61], Y.F. Liang[52], Y.T. Liang[30,61], G.R. Liao[15], L.Z. Liao[48], J. Libby[26], A. Limphirat[58], D.X. Lin[30,61], T. Lin[1], B.J. Liu[1], B.X. Liu[74], C. Liu[33], C.X. Liu[1], D. Liu[19,69], F.H. Liu[51], Fang Liu[1], Feng Liu[6], G.M. Liu[54,i], H. Liu[37,j,k], H.B. Liu[16], H.M. Liu[1,61], Huanhuan Liu[1], Huihui Liu[21], J.B. Liu[69,56], J.L. Liu[70], J.Y. Liu[1,61], K. Liu[1], K.Y. Liu[39], Ke Liu[22], L. Liu[69,56], L.C. Liu[42], Lu Liu[42], M.H. Liu[12,f], P.L. Liu[1], Q. Liu[61], S.B. Liu[69,56], T. Liu[12,f], W.K. Liu[42], W.M. Liu[69,56], X. Liu[37,j,k], Y. Liu[37,j,k], Y.B. Liu[42], Z.A. Liu[1,56,61], Z.Q. Liu[48], X.C. Lou[1,56,61], F.X. Lu[57], H.J. Lu[23], J.G. Lu[1,56], X.L. Lu[1], Y. Lu[7], Y.P. Lu[1,56], Z.H. Lu[1,61], C.L. Luo[40], M.X. Luo[78], T. Luo[12,f], X.L. Luo[1,56], X.R. Lyu[61], Y.F. Lyu[42],

JHEP09(2023)124

F.C. Ma[39], H.L. Ma[1], J.L. Ma[1,61], L.L. Ma[48], M.M. Ma[1,61], Q.M. Ma[1], R.Q. Ma[1,61], R.T. Ma[61], X.Y. Ma[1,56], Y. Ma[45,g], F.E. Maas[19], M. Maggiora[72A,72C], S. Maldaner[4], S. Malde[67], A. Mangoni[28B], Y.J. Mao[45,g], Z.P. Mao[1], S. Marcello[72A,72C], Z.X. Meng[64], J.G. Messchendorp[14,62], G. Mezzadri[29A], H. Miao[1,61], T.J. Min[41], R.E. Mitchell[27], X.H. Mo[1,56,61], N.Yu. Muchnoi[13,b], Y. Nefedov[35], F. Nerling[19,d], I.B. Nikolaev[13,b], Z. Ning[1,56], S. Nisar[11,l], Y. Niu[48], S.L. Olsen[61], Q. Ouyang[1,56,61], S. Pacetti[28B,28C], X. Pan[53], Y. Pan[55], A. Pathak[33], Y.P. Pei[69,56], M. Pelizaeus[4], H.P. Peng[69,56], K. Peters[14,d], J.L. Ping[40], R.G. Ping[1,61], S. Plura[34], S. Pogodin[35], V. Prasad[32], F.Z. Qi[1], H. Qi[69,56], H.R. Qi[59], M. Qi[41], T.Y. Qi[12,f], S. Qian[1,56], W.B. Qian[61], C.F. Qiao[61], J.J. Qin[70], L.Q. Qin[15], X.P. Qin[12,f], X.S. Qin[48], Z.H. Qin[1,56], J.F. Qiu[1], S.Q. Qu[59], C.F. Redmer[34], K.J. Ren[38], A. Rivetti[72C], V. Rodin[62], M. Rolo[72C], G. Rong[1,61], Ch. Rosner[19], S.N. Ruan[42], N. Salone[43], A. Sarantsev[35,c], Y. Schelhaas[34], K. Schoenning[73], M. Scodeggio[29A,29B], K.Y. Shan[12,f], W. Shan[24], X.Y. Shan[69,56], J.F. Shangguan[53], L.G. Shao[1,61], M. Shao[69,56], C.P. Shen[12,f], H.F. Shen[1,61], W.H. Shen[61], X.Y. Shen[1,61], B.A. Shi[61], H.C. Shi[69,56], J.Y. Shi[1], Q.Q. Shi[53], R.S. Shi[1,61], X. Shi[1,56], J.J. Song[20], T.Z. Song[57], W.M. Song[33,1], Y.X. Song[45,g], S. Sosio[72A,72C], S. Spataro[72A,72C], F. Stieler[34], Y.J. Su[61], G.B. Sun[74], G.X. Sun[1], H. Sun[61], H.K. Sun[1], J.F. Sun[20], K. Sun[59], L. Sun[74], S.S. Sun[1,61], T. Sun[1,61], W.Y. Sun[33], Y. Sun[9], Y.J. Sun[69,56], Y.Z. Sun[1], Z.T. Sun[48], Y.X. Tan[69,56], C.J. Tang[52], G.Y. Tang[1], J. Tang[57], Y.A. Tang[74], L.Y. Tao[70], Q.T. Tao[25,h], M. Tat[67], J.X. Teng[69,56], V. Thoren[73], W.H. Tian[57], W.H. Tian[50], Y. Tian[30,61], Z.F. Tian[74], I. Uman[60B], B. Wang[1], B.L. Wang[61], Bo Wang[69,56], C.W. Wang[41], D.Y. Wang[45,g], F. Wang[70], H.J. Wang[37,j,k], H.P. Wang[1,61], K. Wang[1,56], L.L. Wang[1], M. Wang[48], Meng Wang[1,61], S. Wang[12,f], T. Wang[12,f], T.J. Wang[42], W. Wang[57], W. Wang[70], W.H. Wang[74], W.P. Wang[69,56], X. Wang[45,g], X.F. Wang[37,j,k], X.J. Wang[38], X.L. Wang[12,f], Y. Wang[59], Y.D. Wang[44], Y.F. Wang[1,56,61], Y.H. Wang[46], Y.N. Wang[44], Y.Q. Wang[1], Yaqian Wang[18,1], Yi Wang[59], Z. Wang[1,56], Z.L. Wang[70], Z.Y. Wang[1,61], Ziyi Wang[61], D. Wei[68], D.H. Wei[15], F. Weidner[66], S.P. Wen[1], C.W. Wenzel[4], U. Wiedner[4], G. Wilkinson[67], M. Wolke[73], L. Wollenberg[4], C. Wu[38], J.F. Wu[1,61], L.H. Wu[1], L.J. Wu[1,61], X. Wu[12,f], X.H. Wu[33], Y. Wu[69], Y.J. Wu[30], Z. Wu[1,56], L. Xia[69,56], X.M. Xian[38], T. Xiang[45,g], D. Xiao[37,j,k], G.Y. Xiao[41], H. Xiao[12,f], S.Y. Xiao[1], Y.L. Xiao[12,f], Z.J. Xiao[40], C. Xie[41], X.H. Xie[45,g], Y. Xie[48], Y.G. Xie[1,56], Y.H. Xie[6], Z.P. Xie[69,56], T.Y. Xing[1,61], C.F. Xu[1,61], C.J. Xu[57], G.F. Xu[1], H.Y. Xu[64], Q.J. Xu[17], W.L. Xu[64], X.P. Xu[53], Y.C. Xu[76], Z.P. Xu[41], F. Yan[12,f], L. Yan[12,f], W.B. Yan[69,56], W.C. Yan[79], X.Q. Yan[1], H.J. Yang[49,e], H.L. Yang[33], H.X. Yang[1], Tao Yang[1], Y. Yang[12,f], Y.F. Yang[42], Y.X. Yang[1,61], Yifan Yang[1,61], M. Ye[1,56], M.H. Ye[8], J.H. Yin[1], Z.Y. You[57], B.X. Yu[1,56,61], C.X. Yu[42], G. Yu[1,61], T. Yu[70], X.D. Yu[45,g], C.Z. Yuan[1,61], L. Yuan[2], S.C. Yuan[1], X.Q. Yuan[1], Y. Yuan[1,61], Z.Y. Yuan[57], C.X. Yue[38], A.A. Zafar[71], F.R. Zeng[48], X. Zeng[12,f], Y. Zeng[25,h], Y.J. Zeng[1,61], X.Y. Zhai[33], Y.H. Zhan[57], A.Q. Zhang[1,61], B.L. Zhang[1,61], B.X. Zhang[1], D.H. Zhang[42], G.Y. Zhang[20], H. Zhang[69], H.H. Zhang[33], H.H. Zhang[57], H.Q. Zhang[1,56,61], H.Y. Zhang[1,56], J.J. Zhang[50], J.L. Zhang[75], J.Q. Zhang[40], J.W. Zhang[1,56,61], J.X. Zhang[37,j,k], J.Y. Zhang[1], J.Z. Zhang[1,61], Jiawei Zhang[1,61], L.M. Zhang[59], L.Q. Zhang[57], Lei Zhang[41], P. Zhang[1], Q.Y. Zhang[38,79], Shuihan Zhang[1,61], Shulei Zhang[25,h], X.D. Zhang[44], X.M. Zhang[1], X.Y. Zhang[53], X.Y. Zhang[48], Y. Zhang[67], Y.T. Zhang[79], Y.H. Zhang[1,56], Yan Zhang[69,56], Yao Zhang[1], Z.H. Zhang[1], Z.L. Zhang[33], Z.Y. Zhang[74], Z.Y. Zhang[42], G. Zhao[1], J. Zhao[38], J.Y. Zhao[1,61], J.Z. Zhao[1,56], Lei Zhao[69,56], Ling Zhao[1], M.G. Zhao[42], S.J. Zhao[79], Y.B. Zhao[1,56], Y.X. Zhao[30,61], Z.G. Zhao[69,56], A. Zhemchugov[35,a], B. Zheng[70], J.P. Zheng[1,56], W.J. Zheng[1,61], Y.H. Zheng[61], B. Zhong[40], X. Zhong[57], H. Zhou[48], L.P. Zhou[1,61], X. Zhou[74], X.K. Zhou[6], X.R. Zhou[69,56], X.Y. Zhou[38], Y.Z. Zhou[12,f], J. Zhu[42], K. Zhu[1], K.J. Zhu[1,56,61], L. Zhu[33], L.X. Zhu[61], S.H. Zhu[68], S.Q. Zhu[41], T.J. Zhu[12,f], W.J. Zhu[12,f], Y.C. Zhu[69,56], Z.A. Zhu[1,61], J.H. Zou[1], J. Zu[69,56]

[1] *Institute of High Energy Physics, Beijing 100049, People's Republic of China*
[2] *Beihang University, Beijing 100191, People's Republic of China*
[3] *Beijing Institute of Petrochemical Technology, Beijing 102617, People's Republic of China*
[4] *Bochum Ruhr-University, D-44780 Bochum, Germany*
[5] *Carnegie Mellon University, Pittsburgh, Pennsylvania 15213, USA*
[6] *Central China Normal University, Wuhan 430079, People's Republic of China*
[7] *Central South University, Changsha 410083, People's Republic of China*
[8] *China Center of Advanced Science and Technology, Beijing 100190, People's Republic of China*
[9] *China University of Geosciences, Wuhan 430074, People's Republic of China*
[10] *Chung-Ang University, Seoul, 06974, Republic of Korea*
[11] *COMSATS University Islamabad, Lahore Campus, Defence Road, Off Raiwind Road, 54000 Lahore, Pakistan*
[12] *Fudan University, Shanghai 200433, People's Republic of China*
[13] *G.I. Budker Institute of Nuclear Physics SB RAS (BINP), Novosibirsk 630090, Russia*
[14] *GSI Helmholtzcentre for Heavy Ion Research GmbH, D-64291 Darmstadt, Germany*
[15] *Guangxi Normal University, Guilin 541004, People's Republic of China*
[16] *Guangxi University, Nanning 530004, People's Republic of China*
[17] *Hangzhou Normal University, Hangzhou 310036, People's Republic of China*
[18] *Hebei University, Baoding 071002, People's Republic of China*
[19] *Helmholtz Institute Mainz, Staudinger Weg 18, D-55099 Mainz, Germany*
[20] *Henan Normal University, Xinxiang 453007, People's Republic of China*
[21] *Henan University of Science and Technology, Luoyang 471003, People's Republic of China*
[22] *Henan University of Technology, Zhengzhou 450001, People's Republic of China*
[23] *Huangshan College, Huangshan 245000, People's Republic of China*
[24] *Hunan Normal University, Changsha 410081, People's Republic of China*
[25] *Hunan University, Changsha 410082, People's Republic of China*
[26] *Indian Institute of Technology Madras, Chennai 600036, India*
[27] *Indiana University, Bloomington, Indiana 47405, USA*
[28] *INFN Laboratori Nazionali di Frascati, (A)INFN Laboratori Nazionali di Frascati, I-00044, Frascati, Italy; (B)INFN Sezione di Perugia, I-06100, Perugia, Italy; (C)University of Perugia, I-06100, Perugia, Italy*
[29] *INFN Sezione di Ferrara, (A)INFN Sezione di Ferrara, I-44122, Ferrara, Italy; (B)University of Ferrara, I-44122, Ferrara, Italy*
[30] *Institute of Modern Physics, Lanzhou 730000, People's Republic of China*
[31] *Institute of Physics and Technology, Peace Avenue 54B, Ulaanbaatar 13330, Mongolia*
[32] *Instituto de Alta Investigaci'on, Universidad de Tarapac'a, Casilla 7D, Arica, Chile*
[33] *Jilin University, Changchun 130012, People's Republic of China*
[34] *Johannes Gutenberg University of Mainz, Johann-Joachim-Becher-Weg 45, D-55099 Mainz, Germany*
[35] *Joint Institute for Nuclear Research, 141980 Dubna, Moscow region, Russia*
[36] *Justus-Liebig-Universitaet Giessen, II. Physikalisches Institut, Heinrich-Buff-Ring 16, D-35392 Giessen, Germany*
[37] *Lanzhou University, Lanzhou 730000, People's Republic of China*
[38] *Liaoning Normal University, Dalian 116029, People's Republic of China*
[39] *Liaoning University, Shenyang 110036, People's Republic of China*
[40] *Nanjing Normal University, Nanjing 210023, People's Republic of China*
[41] *Nanjing University, Nanjing 210093, People's Republic of China*
[42] *Nankai University, Tianjin 300071, People's Republic of China*

JHEP09(2023)124

[43] National Centre for Nuclear Research, Warsaw 02-093, Poland
[44] North China Electric Power University, Beijing 102206, People's Republic of China
[45] Peking University, Beijing 100871, People's Republic of China
[46] Qufu Normal University, Qufu 273165, People's Republic of China
[47] Shandong Normal University, Jinan 250014, People's Republic of China
[48] Shandong University, Jinan 250100, People's Republic of China
[49] Shanghai Jiao Tong University, Shanghai 200240, People's Republic of China
[50] Shanxi Normal University, Linfen 041004, People's Republic of China
[51] Shanxi University, Taiyuan 030006, People's Republic of China
[52] Sichuan University, Chengdu 610064, People's Republic of China
[53] Soochow University, Suzhou 215006, People's Republic of China
[54] South China Normal University, Guangzhou 510006, People's Republic of China
[55] Southeast University, Nanjing 211100, People's Republic of China
[56] State Key Laboratory of Particle Detection and Electronics, Beijing 100049, Hefei 230026, People's Republic of China
[57] Sun Yat-Sen University, Guangzhou 510275, People's Republic of China
[58] Suranaree University of Technology, University Avenue 111, Nakhon Ratchasima 30000, Thailand
[59] Tsinghua University, Beijing 100084, People's Republic of China
[60] Turkish Accelerator Center Particle Factory Group, (A)Istinye University, 34010, Istanbul, Turkey; (B)Near East University, Nicosia, North Cyprus, 99138, Mersin 10, Turkey
[61] University of Chinese Academy of Sciences, Beijing 100049, People's Republic of China
[62] University of Groningen, NL-9747 AA Groningen, The Netherlands
[63] University of Hawaii, Honolulu, Hawaii 96822, USA
[64] University of Jinan, Jinan 250022, People's Republic of China
[65] University of Manchester, Oxford Road, Manchester, M13 9PL, United Kingdom
[66] University of Muenster, Wilhelm-Klemm-Strasse 9, 48149 Muenster, Germany
[67] University of Oxford, Keble Road, Oxford OX13RH, United Kingdom
[68] University of Science and Technology Liaoning, Anshan 114051, People's Republic of China
[69] University of Science and Technology of China, Hefei 230026, People's Republic of China
[70] University of South China, Hengyang 421001, People's Republic of China
[71] University of the Punjab, Lahore-54590, Pakistan
[72] University of Turin and INFN, (A)University of Turin, I-10125, Turin, Italy; (B)University of Eastern Piedmont, I-15121, Alessandria, Italy; (C)INFN, I-10125, Turin, Italy
[73] Uppsala University, Box 516, SE-75120 Uppsala, Sweden
[74] Wuhan University, Wuhan 430072, People's Republic of China
[75] Xinyang Normal University, Xinyang 464000, People's Republic of China
[76] Yantai University, Yantai 264005, People's Republic of China
[77] Yunnan University, Kunming 650500, People's Republic of China
[78] Zhejiang University, Hangzhou 310027, People's Republic of China
[79] Zhengzhou University, Zhengzhou 450001, People's Republic of China

[a] Also at the Moscow Institute of Physics and Technology, Moscow 141700, Russia
[b] Also at the Novosibirsk State University, Novosibirsk, 630090, Russia
[c] Also at the NRC "Kurchatov Institute", PNPI, 188300, Gatchina, Russia
[d] Also at Goethe University Frankfurt, 60323 Frankfurt am Main, Germany
[e] Also at Key Laboratory for Particle Physics, Astrophysics and Cosmology, Ministry of Education; Shanghai Key Laboratory for Particle Physics and Cosmology; Institute of Nuclear and Particle Physics, Shanghai 200240, People's Republic of China
[f] Also at Key Laboratory of Nuclear Physics and Ion-beam Application (MOE) and Institute of Modern Physics, Fudan University, Shanghai 200443, People's Republic of China
[g] Also at State Key Laboratory of Nuclear Physics and Technology, Peking University, Beijing 100871, People's Republic of China
[h] Also at School of Physics and Electronics, Hunan University, Changsha 410082, China

JHEP09(2023)124

[i] *Also at Guangdong Provincial Key Laboratory of Nuclear Science, Institute of Quantum Matter, South China Normal University, Guangzhou 510006, China*
[j] *Also at Frontiers Science Center for Rare Isotopes, Lanzhou University, Lanzhou 730000, People's Republic of China*
[k] *Also at Lanzhou Center for Theoretical Physics, Lanzhou University, Lanzhou 730000, People's Republic of China*
[l] *Also at the Department of Mathematical Sciences, IBA, Karachi, Pakistan*